

ASML

Advanced Cable Testing for ASML Lithography Machines

The City College of New York



Grove School of Engineering

Department of Mechanical Engineering

Professor: Ali Sadegh Ph.D.

Sponsor: ASML

Supervisor: Matthew Sorna, PE

Group 3:

OLEKSIY BRYHADYR, PHILIP CZUDAK, HUSSEIN NAJDE, FRAYLIN SANCHEZ GIL,
ISHVAR SITALDIN, AHMED TARIQ

5/20/2025

Table of Contents

ABSTRACT.....	5
NOMENCLATURE.....	6
INTRODUCTION.....	7
BACKGROUND	7
PROJECT DESCRIPTION	8
MOTIVATION	8
LITERATURE SEARCH	8
<i>General information</i>	9
<i>Static Analysis - 4 Point Bending</i>	10
<i>Dynamic Analysis – Semicircular Cable Assembly</i>	12
PROBLEM STATEMENT	16
OBJECTIVES	16
SPECIFICATIONS AND REQUIREMENTS.....	16
STEPS TAKEN	16
GANTT CHART AND TIMETABLE.....	18
DESIGN CONCEPTS.....	20
STATIC DESIGN.....	20
<i>Four-Point Bend Test Design</i>	20
DYNAMIC DESIGNS.....	21
<i>Design Requirements</i>	21
<i>Design Iteration 1</i>	22
<i>Design Iteration 2</i>	23
<i>Design Iteration 3</i>	24
<i>Design Iteration 4</i>	25
<i>Evaluation of Iterations</i>	26
<i>Final Design Choice</i>	28
ANALYSIS OF DESIGN.....	29
STRUCTURE	30
BELT-DRIVEN LINEAR ACTUATOR	31
SENSING MECHANISM	31
CLAMPING MECHANISM	32
TEST FIXTURE WITHOUT ENCLOSURE	32
SYSTEM CIRCUIT DIAGRAMS AND WIRING CONFIGURATION.....	33
SYSTEM OPERATION BREAKDOWN.....	35

RESULTS	37
RESULTS OF FINITE ELEMENT ANALYSIS	37
RESULTS OF FOUR-POINT BEND TEST	37
<i>Trial 1</i>	37
<i>Trial 2</i>	38
RESULTS OF THE DYNAMIC TEST	39
<i>Trial 1</i>	40
<i>Trial 2</i>	41
<i>Trial 3</i>	42
<i>Trial 4</i>	43
<i>Trial 5</i>	44
DISCUSSION OF RESULTS	46
SUMMARY AND RECOMMENDATIONS.....	48
CONCLUSION.....	48
REFERENCES.....	49
APPENDIX.....	51
APPENDIX A (ARDUINO CODE)	51
APPENDIX B (MATLAB CODE)	55

Abstract

To support ASML's development of high-precision lithography systems, this project quantified the bending stiffness of a flat conductor cable (FCC) subjected to extreme dynamic acceleration. Analytical methods alone were insufficient due to the cable's complex geometry. A four-point bend test was designed for static analysis, while a dynamic test fixture simulated in-service conditions using a fixed-fixed semicircular setup with force sensing. Static testing yielded an average bending stiffness of $2.605 \times 10^5 \text{ N}\cdot\text{mm}^2$, while dynamic trials returned $1.419 \times 10^5 \text{ N}\cdot\text{mm}^2$. The agreement between methods validated the experimental setups. These results provide ASML with actionable mechanical data to improve cable reliability, minimize wear, and enhance performance under high-stress operating conditions.

Nomenclature

Symbol	Meaning
β	Bending Stiffness
σ	Flexural Stress
ε	Flexural Strain
E	Young's Modulus
U	Strain Energy
W	Work
F	Force Applied
L	Support Span
D	Midspan deflection
h	Height
w	Width
M	Bending Moment
I	Second Moment of Inertia
δ	Change in Position of Beam Midpoint
d_{HA}	Horizontal Displacement of Arch
d_{VA}	Vertical Displacement of Arch
c_A	Rotation of Arch
B_{ij}	Stiffness Coefficients
H_A	Horizontal Reaction Force
V_A	Vertical Reaction Force
M_A	Reaction Moment
R	Radius of Curvature

Introduction

Background

In 1984, Advanced Semiconductor Materials Lithography emerged from a joint venture between Philips and ASM International. Known today as ASML, the company has enjoyed immense success, expanding its operations to offices worldwide and employing over 44,000 employees [1]. From humble beginnings, the company has established itself as one of the world's leading chip-making equipment manufacturers. Without ASML's machines, the most recognizable names in tech, such as Intel or TSMC, would not continue their operations and manufacture the millions of microchips needed to keep life moving forward [2].

Although ASML has diversified its product lineup with metrology equipment, it is deeply rooted in lithography systems [3]. Lithography is typically the first stage of silicon wafer processing. Formally known as photolithography, this process projects UV light through a mask containing the desired patterns onto wafers covered in thin photoresist films. The induced chemical process transfers patterns carried by light onto the wafer and allows for further steps such as deposition or etching [4].

Most innovations within lithography systems involve speed, volume, and above all else, resolution. While ASML offers industry-standard deep ultraviolet (DUV) systems (enabling feature sizes of 38nm) [5], their latest innovation, extreme ultraviolet (EUV) systems (enabling feature sizes of 8nm) [6], looks to uphold Moore's Law for as long as possible. The contributing factor for such increased resolutions is the fourteen times shorter wavelengths EUV systems can output [5].

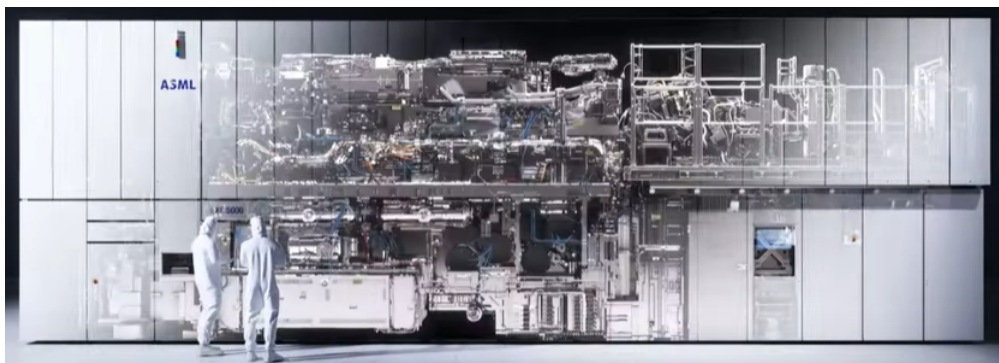


Figure 1 - Internal and external views of ASML's newest EXE systems along with humans for scale.

Taking their 'EXE' system to the peak of innovation required optimizing an additional aspect: speed. Single wafers may have to be patterned hundreds of times before being diced into chips, a potentially lengthy process. Maximizing the output of their machines, measured in wafers per hour, ASML developed a reticle that accelerates linearly at 32g; for perspective, a car experiencing this acceleration would go from 0 to 60 mph in less than a tenth of a second [7]. Completing this action requires a significant amount of power and vacuum; currently, a robust FCC array with integrated hose lines is fixed onto the top of the optic bay and looped down to the magnetic reticle stage. This cable undergoes a continuous yet erratic rolling bend while the machine operates.

Project Description

Our team was tasked with determining the bending stiffness of the cables supplied in collaboration with analysis engineers from ASML. Data collected from our tests would further the company's modeling capabilities and analysis. Such data is fundamental in diagnosing flaws and verifying future improvements. Meeting the strict accuracy requirements for projects of such magnitude required acquiring and comparing data from static and dynamic tests. In turn, the team worked on supplying testing equipment for both cases.

Apart from the industry-specific aspect of this project, it serves as our senior design capstone project. The academic goal of the class was to experience every aspect of the product development cycle that competent engineers must adhere to. Only being given an overall goal by ASML, the team had to develop novel concepts, evaluate feasibility, generate and validate designs against desired outcomes, manufacture prototypes, and run tests before presenting the final product. Facing the complex challenges that arise at the intersection of engineering analysis and product development provided a rite of passage for our team.

Motivation

To maintain market dominance and uphold its reputation, ASML must ensure its machines run as intended for as long as possible. In the semiconductor industry, downtime (specifically unplanned downtime) for any machine results in significant losses and frustration. Business Korea reported that in 2020, a Samsung factory lost over 43 million dollars because of a 30-minute power outage [8]. Apart from total failure, downtime may occur from the malfunction of a single component. ASML engineers suspect the robust nature of their power cables in combination with extreme accelerations may lead to early degradation, compromising their effectiveness.

Integrated circuits must be manufactured with nanometer precision; therefore, all nanofabrication facilities are cleanrooms. These specialized facilities constantly filter air through HEPA filters to minimize the risk of particles contaminating the wafer surface. Federal standards designate clean rooms by class, each determined by the particle concentration per cubic foot of air [9]. To minimize contamination and comply with the cleanroom environment, ASML's machines operate under vacuum. Unfortunately, the necessary conditions for producing chips are at risk if these cables rapidly degrade; determining the bending stiffness of such cables provides invaluable data for amending the issue. Rectifying potential problems before they cause a rift between customer and supplier will sustain the powerful relationships propelling ASML forward.

Literature Search

The main benefit of a literature search is optimizing time and resources; gaining a deeper understanding of the problem and possible solutions minimizes potential errors. Before generating concepts and drafting designs, our team investigated four main topics: cable characteristics, material properties, static test methodology, and existing dynamic test equipment. Gauging common cable characteristics and their impact on properties such as bending stiffness against the cables supplied by ASML laid the groundwork for our intuition of the magnitude of forces we may be dealing with. Pairing classroom knowledge with external sources relating material properties with stress, strain, and force was key in directing us towards the equations we would need to apply when manipulating future data. Likewise, evaluating patents for existing static and dynamic wire testing equipment aided our decision-making process when designing our innovative solution.

General information

Manufacturers enhance power cable designs by considering various factors, weighing each advantage and trade-off against the intended application. In ASML's case, flexibility is a critical limiting factor. Thus, examining the conductive core, insulating material, and overall construction is essential. There are two types of conductive cores: stranded and solid. Stranded wires are more expensive; however, they offer greater flexibility and longer flex lives in motion applications [10].

PVC and PTFE are the most commonly used insulation materials. PTFE, also known as Teflon, is favored in high-performance applications due to its exceptional thermal, chemical, and electrical stability. Although less durable, PVC is widely used for household applications because of its low cost and superior flexibility [11]. The round cable construction offers beneficial properties that improve reliability against mechanical stress, yet FCCs provide greater flexibility [12]. The FCC, with a stranded core and PTFE insulation supplied for testing, incorporates thoughtful design considerations, although questions remain about whether the supplier optimized it for the expected conditions.

Bending stiffness (EI) measures a cable's resistance to bending, which is crucial for its performance under cyclic loading. According to the CIGRE B1 Technical Brochure, Reference 862, this stiffness property is defined by the relationship between the bending moment and curvature, often exhibiting non-linear behavior [13]. Specifically, as the curvature applied to a cable increases, the stiffness increases until plastic deformation occurs. Besides a cable's geometry, key factors influencing the stiffness include magnitude, temperature, bending rate, and amplitude [13]. An accurate assessment of overall bending stiffness is essential, providing critical insights into a cable's durability under operational stresses.

The ANSI/NEMA WC53/ICEA T-27-581-2020 standard further supports this characterization by outlining standard physical tests for insulated cables, especially in Section 4 – Physical Methods [14]. While this standard does not specifically measure bending stiffness or modulus values, it includes methods for assessing mechanical durability and deformation resistance. Sections 4.2 (Cold Bend) and 4.4 (Flexibility Test for Interlocked Armor) evaluate the integrity of cables when subjected to flexing and bending conditions [14]. These qualitative tests confirm whether a cable can endure repeated or extreme bending without fracturing or cracking.

Section 4.3 (Heat Deformation) also details tests that expose cables to compressive loads at elevated temperatures, demonstrating the extent of permanent deformation that occurs under thermal-mechanical stress [14]. While these tests do not provide direct measurements of stiffness or modulus, they offer insights into how material stiffness evolves in thermally active environments. Section 4.11 (Tensile Strength, Stress, and Elongation Tests) presents a standardized procedure for stretching cable components to the point of failure. By collecting stress-strain data throughout these tests, Young's modulus (E) can be derived using Hooke's Law in the linear elastic region [14].

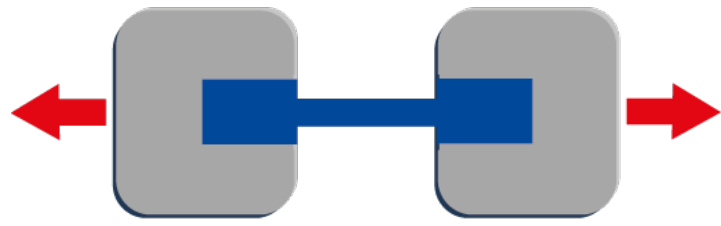


Figure 2 - Tensile Test Setup.

Overall, these physical methods create a consistent framework for indirectly assessing the mechanical resilience and deformation resistance of cables, serving as a foundation for our quantitative approaches.

Static Analysis - 4 Point Bending

Bending stiffness is commonly evaluated using three-point and four-point bending tests. The three-point bending method applies a central load between two supports, creating a bending moment with a non-uniform stress distribution. While this method is suitable for initial analysis, its accuracy is limited due to uneven force application.

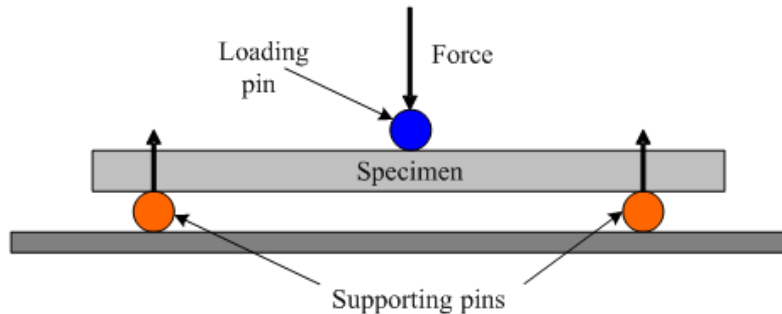


Figure 3 - Three-Point Bend Test Setup.

We will conduct a four-point bending test following ASTM D6272 to accurately quantify the FCC's bending stiffness. This test setup will establish a region with a constant bending moment and zero shear between the inner loading points, creating ideal conditions for flexural characterization.

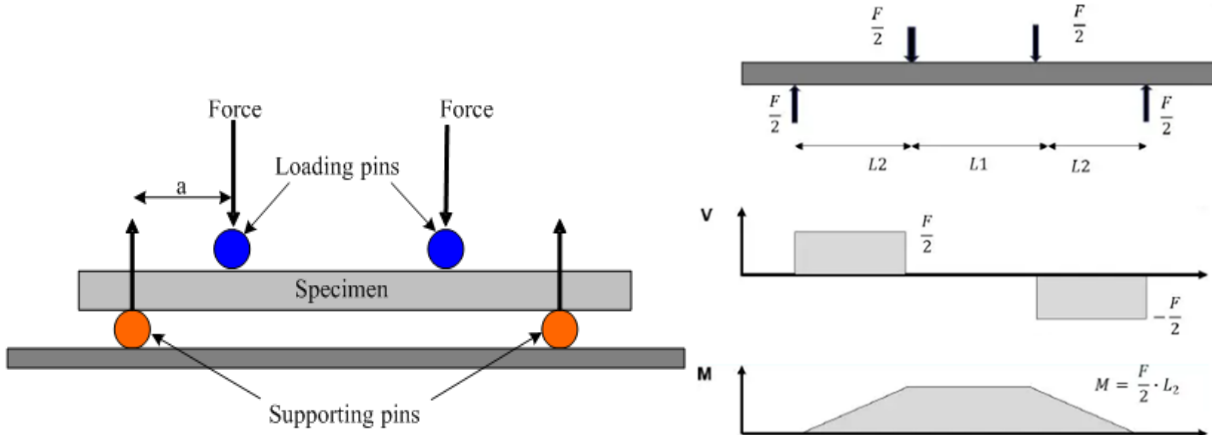


Figure 4 – Four-Point Bend Test Setup. (From Top to Bottom) Free Body, Shear Force and Bending Moment Diagrams.

Following ASTM conventions, where the load span equals half the support span, we will calculate the maximum outer fiber stress and the midspan strain. These calculations will allow us to determine Young's modulus using Hooke's Law [15]:

$$\text{Eq (1): } \sigma = \frac{3FL}{4h^2w}$$

$$\text{Eq (2): } \varepsilon = \frac{hD}{0.23L^2}$$

$$\text{Eq (3): } E = \frac{\sigma}{\varepsilon}$$

With Young's modulus known, we will be able to calculate the bending stiffness:

$$\text{Eq (4): } I = \frac{wh^3}{12}$$

$$\text{Eq (5): } \beta = EI$$

This approach will enable us to derive bending stiffness based on fundamental beam mechanics while adhering to ASTM's elastic limit guidelines, which allow for strains of up to 5%. Unlike simplified flexural stiffness formulas that rely solely on load and deflection, this method will rigorously capture the material-specific elastic response and geometry.

Although TAPPI/ANSI T 836 utilizes a moment-based stiffness equation tailored for corrugated materials, its procedures reinforce our assumptions: small-deflection conditions, delayed deflection readings, and careful span and clamp control are critical for ensuring repeatability and accuracy [15][16]. The standard emphasizes allowable strain ranges and deflection precision, further supporting the validity of our method across composite and flexible cable-like structures.

In summary, this analytical framework, rooted in ASTM D6272 and supported by TAPPI T 836, provides a consistent and validated approach for determining flexural stiffness in the cable

system. The EI values obtained serve as essential input for both static deflection modeling and dynamic system response analysis in the project's later phases.

Dynamic Analysis – Semicircular Cable Assembly

Just like with the 4-point static test, this study aims to obtain the effective bending stiffness of the cable. The difference between the dynamic and static analyses is that the cable is in a semicircular curved state and is experiencing a displacement on one of the ends. This dynamic configuration was inspired by standard cable fatigue tests commonly utilized in industrial validation. Among these tests, the C-Track and Tick-Tock tests are frequently employed to simulate repetitive bending in motion systems. The C-Track test subjects cables to guided bending through carriers, while the Tick-Tock test uses a pendulum-style motion to bend the cable around a fixed mandrel repeatedly [17]. While both methods are designed to assess fatigue life, they do not provide quantitative insights into cable stiffness.

Our team was particularly influenced by the Rolling Bend Test, which eliminates fixed-radius supports and allows for unsupported, continuous flexing. This method lets the cable bend freely and naturally distribute strain along its length [18]. This approach closely resembles the conditions our semicircular test assembly would be designed to replicate. By modifying this concept to incorporate force sensing at the fixed boundary, we transformed a fatigue-oriented protocol into a tool for measuring mechanical stiffness, a critical parameter for modeling deformation in high-precision environments.

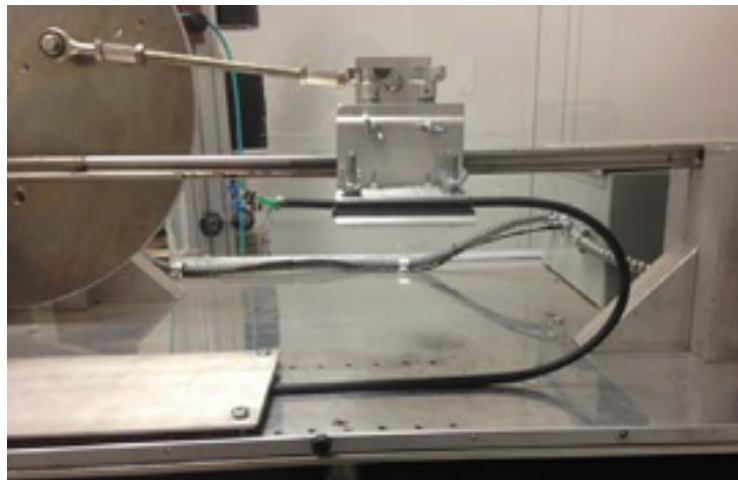


Figure 5 - Rolling Bend Test Setup [18]

In this case the cable was configured into a fixed-fixed semicircular arch with a known radius of 75mm. Knowing this setup, an experimental approach combined with theoretical analysis based on established structural mechanics principles was adopted.

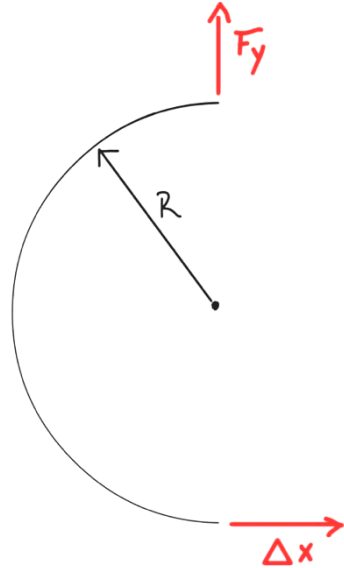


Figure 6 - Sketch of Semicircular cable setup for Dynamic Analysis.

The analytical foundation for this method was sourced from **Roark's Formulas for Stress and Strain (7th Edition), Chapter 9, Table 9.3**, titled "Reaction and deformation formulas for circular arches." This table provides comprehensive solutions for various arch configurations and loading conditions. The experimental setup corresponds to **Case 5: "Left end fixed, right end fixed"** within this table.

5. Left end fixed, right end fixed



Figure 7 - Case 5 in Roark's Formulas for Stress and Strain (7th Edition), Chapter 9, Table 9.3, titled "Reaction and deformation formulas for circular arches."

Roark's provides a set of general deformation equations for this case, which relate the displacements (d_{HA} , d_{VA}) and rotation (c_A) at one end of the arch (denoted as end A) to the corresponding reaction forces (H_A , V_A) and moment (M_A) at that same end. These equations incorporate stiffness/compliance coefficients (B_{ij}), which are functions of the arch's geometry (specifically the half-angle ψ) and factors k_1 , k_2 that account for hoop stress and shear deformation [19]. The general form of these equations is:

- $d_{HA} = \frac{R^3}{EI} \left(B_{HH}H_A + B_{HV}V_A + B_{HM} \frac{M_A}{R} - LFH \right)$
- $d_{VA} = \frac{R^3}{EI} \left(B_{VH}H_A + B_{VV}V_A + B_{VM} \frac{M_A}{R} - Lfv \right)$
- $c_A = \frac{R^2}{EI} \left(B_{MH}H_A + B_{MV}V_A + B_{MM} \frac{M_A}{R} - LfM \right)$

Here, LFH , Lfv , and LfM are terms that depend on any externally applied loads.

It's important to note that Roark's standard diagrams for arches orient the baseline (the line connecting the supports) horizontally. In our physical setup, the U-shape of the arch opens to the right, meaning the line connecting the two fixed clamps is vertical. This requires a careful mapping of our physical displacements and forces to Roark's terminology. The specific conditions substituted into Roark's general equations for end A were:

- **Arch Geometry:**

The arch is a semicircle, so its half-angle $\psi=\pi/2$ radians (90°)

- **Applied Displacement at End A (e.g., the "bottom" moving clamp in your setup):**

The motor applies a physical horizontal displacement, $\Delta x_{\text{physical}}$. Due to our setup's orientation (U-shape opening to the right, line of supports is vertical), this physical horizontal displacement is perpendicular to Roark's arch baseline. Thus, it corresponds to Roark's vertical displacement at end A: $d_{VA} = \Delta x_{\text{physical}}$

- **Other Constraints at End A:**

- The physical displacement along the line of supports (Roark's horizontal displacement) is zero: $d_{HA}=0$
- The rotation at the fixed end A is zero: $c_A=0$

- **Measured Reaction Force:**

We are measuring the physical vertical force, $F_{y,\text{physical}}$, which in this orientation is along Roark's arch baseline. This is being measured at the other fixed end (end B), it corresponds to Roark's horizontal reaction force at end B: $HB = F_{y,\text{physical}}$ (The derivation will solve for HA, and then $HB = -HA$ due to overall horizontal equilibrium).

- **External Loads:**

No external loads are applied during this specific test, so the load terms $LFH=0$, $LFV=0$, $LMF=0$.

- **Simplification:** For this analysis, the minor effects of hoop stress and shear deformation were neglected, meaning Roark's correction factors k_1 and k_2 were approximated as 1.

These specific conditions, when substituted into Roark's general system of three deformation equations for Case 5 (along with the B_{ij} coefficients for $\psi=\pi/2$), allow the system to be solved algebraically for the reactions at end A (HA, VA, MA). From HA, we find HB (= $F_{y,\text{physical}}$) in terms of the applied d_{VA} (= $\Delta x_{\text{physical}}$), the radius R, and the bending stiffness EI_{eff} [19].

With these conditions (physical horizontal displacement $\Delta x_{\text{physical}}$ corresponding to Roark's d_{VA} at end A, other displacements/rotations at A being zero, and no external loads), the specific values for the B_{ij} coefficients for a semicircle ($\psi=\pi/2$, $k_1=k_2=1$) were determined as (e.g., $B_{HH} = \pi/2$, $B_{HV} = 2$, etc.). Substituting these coefficients and the specific displacement conditions ($d_{HA} = 0$, $d_{VA} = \Delta x_{\text{physical}}$, $c_A = 0$) into the general deformation equations transformed them into a solvable system of three linear algebraic equations with HA, VA, and MA as the unknown reactions at end A.

This system was then solved algebraically for the **horizontal reaction force HA** (which corresponds to the negative of the physical vertical force $F_{y,\text{physical}}$ measured at the other fixed end B, i.e., $HA = -HB = -F_{y,\text{physical}}$, or directly to $F_{y,\text{physical}}$ if measured at end A with appropriate sign convention) in terms of the applied physical horizontal displacement $\Delta x_{\text{physical}}$ (which is d_{VA} in

Roark's frame), the radius R, and the bending stiffness EI_{eff} . The algebraic solution of the system of equations yielded the following relationship for the magnitude of the horizontal reaction force $|H_A|$ (and thus $|H_B|$):

$$|H_A| = |H_B| = \left(\frac{16}{72 - \pi^2} \right) \frac{EI_{eff}}{R^3} \cdot |\Delta x_{physical}|$$

This equation was then rearranged to solve for the effective bending stiffness:

$$EI_{eff} = \left(\frac{72 - \pi^2}{16} \right) \frac{|H_B|}{|\Delta x_{physical}|} \cdot R^3$$

Replacing $|H_B|$ with our physically measured vertical force $|F_{y,physical}|$ and $|\Delta x_{physical}|$ with our physically applied horizontal displacement, the formula remains:

$$EI_{eff} = \left(\frac{72 - \pi^2}{16} \right) \frac{|F_{y,physical}|}{|\Delta x_{physical}|} \cdot R^3$$

The dimensionless constant $K = (72 - \pi^2)/16$ is approximately 3.883. Thus, the final working formula used to determine the bending stiffness from the experimental data, based on Roark's formulas, is:

$$EI_{eff} = 3.883 \frac{|F_{y,physical}|}{|\Delta x_{physical}|} \cdot R^3$$

Problem Statement

Objectives

The primary objective of the project is to determine the bending stiffness properties of the cable that are driven by the unique geometry and composition of the cable array. As previously stated, bending stiffness refers to a material's resistance to bending deformations under an external force. This property is characterized by the material's Young's modulus and the structural second moment of inertia of the cross-section. To begin, the cable array is composed of copper stranding and polytetrafluoroethylene, or PTFE, insulation. Although copper is a widely used and understood material, the stranded layout creates complications in the bending properties due to friction between the strands. Additionally, the anisotropic nature of PTFE creates further challenges in the ability to approximate the bending stiffness. With all this in mind, the project scope was to determine the best experimental method to measure the bending stiffness or bending modulus.

Specifications and Requirements

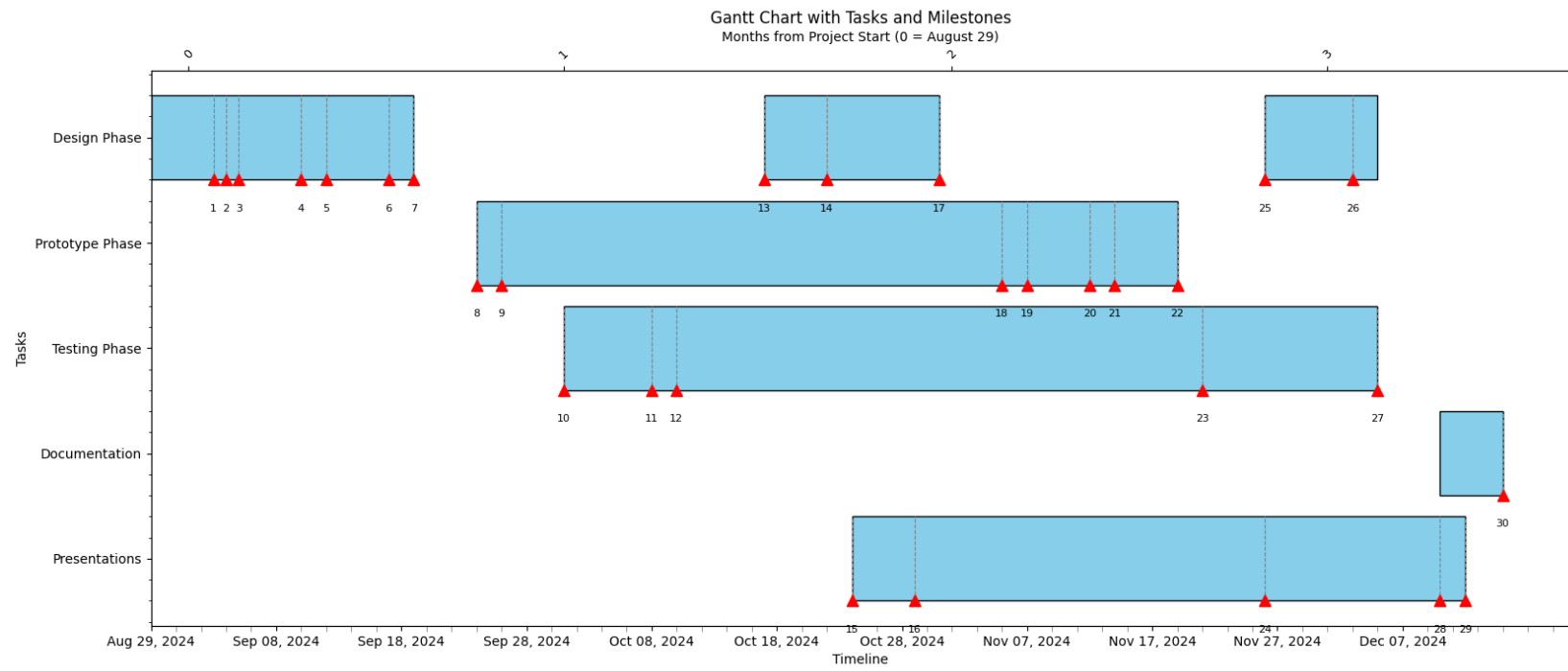
A cable array with dimensions 600 x 115 x 4 mm is attached to a moving plate that is accelerated up to $313 \frac{m}{s^2}$, causing the cable to deform unexpectedly and experience friction with the surroundings. Over time, this friction causes wear and tear on the cable, ejecting particulates into the system and potentially contaminating the product. These issues would increase the frequency of maintenance and repairs, increasing cost and lowering reliability. As a result, the client has requested a thorough investigation of the cable array and its structural properties. They hope to use the data to develop an improved cable design and prevent these issues from arising.

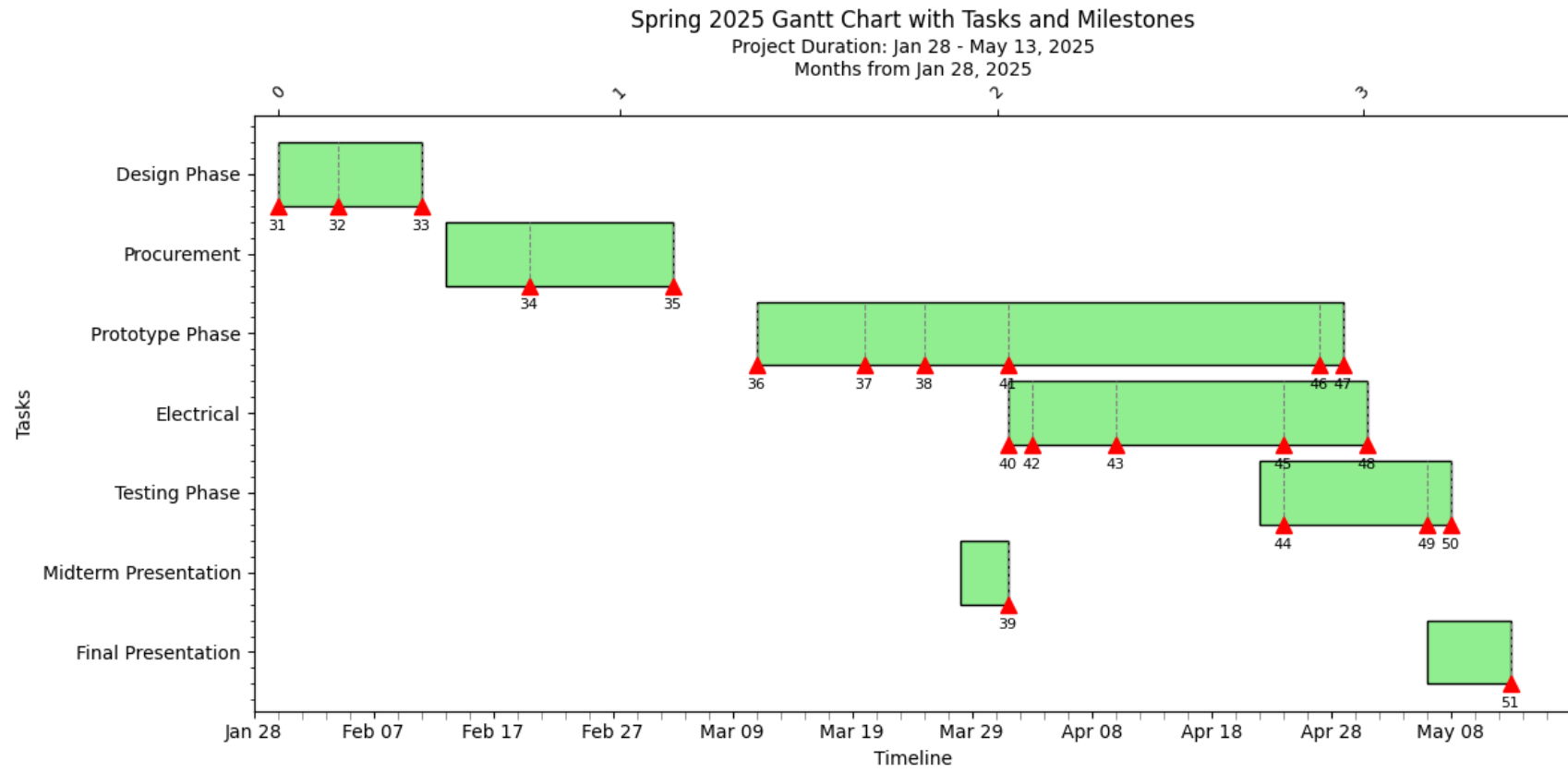
Steps Taken

To determine the cable properties, the team began their work by recreating the cable in SolidWorks. Next, the team focused on researching existing literature on cables and the methodology used to test them. After some examinations, we decided to use the standard 4-point bend test as the static design. Using the CAD model, we ran preliminary simulations to obtain stress, displacement, and ultimately the bending modulus using the 4-point bend test. Then, we conducted an identical experiment using the physical cable and 3D printed parts that served as the support and loading arms. After running a couple of trials, we plotted the stress vs. strain curves and obtained the bending modulus. Then, the focus shifted to a dynamic design approach. Using previously acquired knowledge regarding the various setups, we developed a dynamic test stand after several design iterations. Lastly, we manufactured the dynamic test stand, conducted measurement experiments, collected the data, and compared it with the data from the static test stand.

Milestone Number	Milestone Description	Completion Date
1	Team Formation and Role Assignment	09/03/24
2	Project Scope and Objective Selection	09/04/24
3	Initial Brainstorming and Literature Review	09/05/24
4	Sponsor Meeting to Define Requirements	09/10/24
5	Development of Testing Methodology Options	09/12/24
6	Finalization of Four-Point Bend Test Methodology	09/17/24
7	Conceptual Design of Dynamic Stand Prototypes	09/19/24
8	CAD Modeling Initiated for Cable	09/24/24
9	Optimization of Cable Design for Simulation	09/26/24
10	Finite Element Analysis (FEA) Setup Initiated	09/27/24
11	Review and Refinement of Static Test Designs	09/30/24
12	FEA Beam Element Integration for Simulation	10/01/24
13	Preliminary Dynamic Stand Component Analysis	10/03/24
14	Finalized Initial Dynamic Stand Prototype Design	10/07/24
15	Drafted Peer Review Presentation	10/09/24
16	Delivered Peer Review Presentation	10/10/24
17	Refinement of Three-Point and Four-Point Test Concepts	10/18/24
18	Technical Consultation with Mr. Chen	10/20/24
19	Procurement of Materials for Four-Point Bend Test	10/27/24
20	Fabrication of Testing Cable Prototype	10/29/24
21	Refinement of Prototype Manufacturing Process	11/01/24
22	Completion of Cable Prototype and Component Printing	11/04/24
23	Assembly of Four-Point Bend Test Set	11/14/24
24	Sponsor Presentation on Preliminary Results	11/26/24
25	Introduction of New Design Concepts (3 and 4)	12/06/24
26	Final Selection of Design Concept (Design 4)	12/13/24
27	Execution of Four-Point Bend Test	12/18/24
28	Final Presentation Preparation	12/20/24
29	Final Presentation Delivered	12/21/24
30	Final Report Compilation and Submission	12/23/24
31	Cable Bend Curve Modeling Discussion	01/30/25
32	Base Motion System Design Discussion	02/04/25
33	Force Sensor Selection and Integration Plan	02/11/25
34	Started Looking for Materials to Order	02/20/25
35	Bill of Materials Finalized and Submitted	03/04/25
36	Material Verification and Cutting Preparation	03/11/25
37	Aluminum Cutting and Tapping Completed	03/20/25
38	Initial Assembly and Adjustment of Structure	03/25/25
39	Midterm Presentation Delivered	04/01/25
40	Wiring and Voltage Setup	04/01/25
41	Frame Manufacturing and Insert Installation	04/01/25
42	Arduino Code Developed for Basic Motion	04/03/25
43	Motor Control Testing and Calibration	04/10/25
44	Limit Switch and Gantry Testing	04/24/25
45	Arduino Motion Control Improved with Limit Switches	04/24/25
46	Acrylic Mounting and Cable Clamping	04/27/25
47	Cable Mounting System Fully Installed	04/29/25
48	Successful Working Website Interface	05/01/25
49	Testing Loop Motion Calibration Completed	05/06/25
50	System Calibration and Data Collection	05/08/25
51	Final Presentation Delivered	05/13/25

Gantt Chart and Timetable





Design Concepts

Static Design

Four-Point Bend Test Design

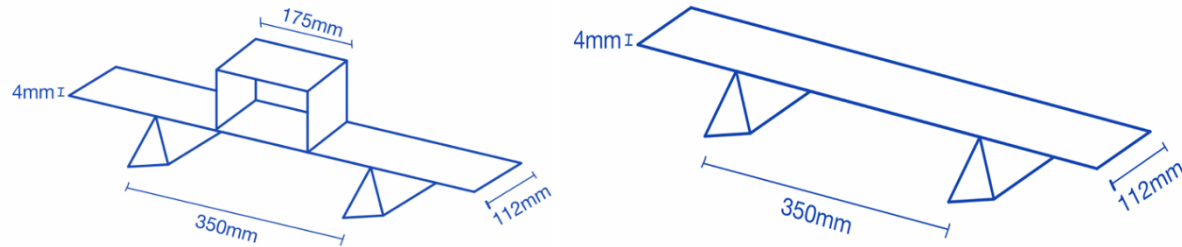


Figure 8 - Dimensions of Four-Point Bend Test Setup.

The four-point bend test fixture was custom-designed and fabricated using accessible components to simulate the required boundary conditions. The setup included:

- **3D Printed Supports:** These were designed to hold the cable at three critical locations. Two outer supports fixed the ends of the cable, while a central support bracket applied the load across two inner contact points.
- **Adjustable U-Bracket:** A U-shaped 3D printed bracket was used to apply force evenly across the span between the inner supports. This bracket served as a platform to add incremental loads (weights), ensuring symmetrical application of force.
- **Dial Gauge:** Positioned directly beneath the midpoint of the cable, this tool recorded vertical deflection as weights were added.
- **Wooden Base:** The supports and gauge were mounted on a wooden base to ensure a stable and vibration-free testing environment.

This setup allowed for precise adjustment of load positions and ensured repeatable measurements across multiple trials.

Fabrication and Assembly

The 3D printed supports were designed in SolidWorks and printed using PLA filament. The dimensions of the supports were matched to the cable's width to prevent lateral shifting during loading. The U-bracket height was made adjustable to accommodate different cable thicknesses and deflection ranges. The dial gauge was zeroed before each test to ensure consistent measurements.

The setup was calibrated to maintain a constant inner support span, and force was applied in increments, allowing for multiple data points to be collected and averaged for higher accuracy.

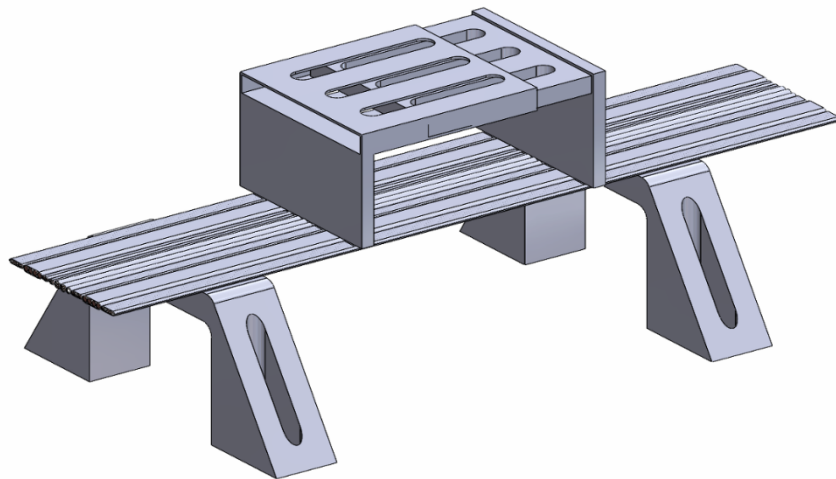


Figure 9 - SolidWorks model of Four-Point Bend Test Setup

Dynamic Designs

Design Requirements

The dynamic test fixture must be designed specifically for linear motion, as the test only requires controlled horizontal displacement of the cable's bottom end. The top end of the cable must remain fixed throughout the test to simulate real-world conditions where one end of the cable is anchored while the other experiences movement. To effectively evaluate cable performance under such conditions, the bottom base of the fixture must be capable of translating at least 300 mm. This travel range is essential to apply sufficient mechanical strain and observe the cable's response to extended linear displacement, such as stretching, fatigue, or failure under repeated motion. Additionally, the fixture must maintain a vertical distance of 150 mm between the mounting plates where the cable is secured. This spacing ensures that the cable is held with proper tension and alignment, providing a realistic representation of installation conditions while preventing slack that could interfere with test results. Finally, the fixture must be compatible with cables of at least 600 mm in length. This allows enough cable to accommodate both the fixed and moving ends, the vertical plate spacing, and the travel distance, while also enabling accurate analysis of bending radii, material behavior, and fatigue performance over a substantial length. These design parameters are critical to ensure the fixture aligns with the company's testing standards and provides reliable, reproducible results.

Design Iteration 1

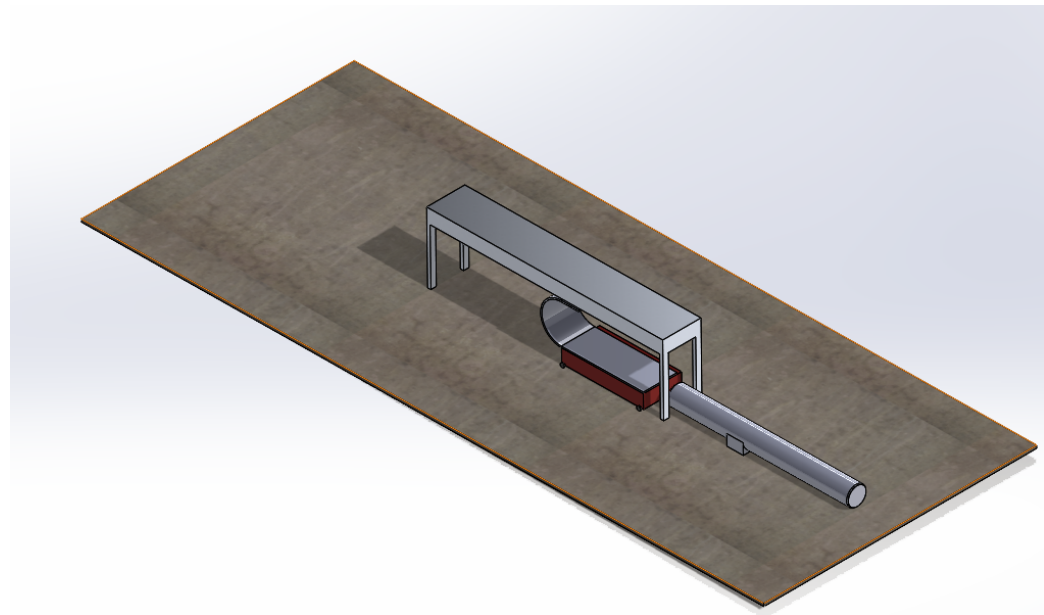


Figure 10 - Design Concept #1 for the Dynamic Test Fixture.

Our initial design concept was developed based on the core principles discussed for the dynamic testing setup. In this approach, the cable is pre-bent to match a vertical plate-to-plate spacing of 150 mm and is securely clamped at both ends, fixed at the top plate and attached to a movable base at the bottom. The key objective of this setup is to measure the force exerted by the cable on the fixed top plate. To achieve this, a force sensor is incorporated at the top, which continuously captures data throughout the testing process. Continuous data output is essential due to the dynamic nature of the test, where the bottom base moves back and forth to simulate real operating conditions similar to those inside ASML's lithography machines.

The motion of the bottom base is achieved using a linear actuator, which drives the platform to oscillate horizontally, fully extending and contracting the 600 mm cable. To allow for this, the bottom base must move at least 300 mm from its starting position. This displacement ensures the cable undergoes its full range of motion, enabling comprehensive analysis of the forces it generates during operation. The base is mounted on four small wheels to allow horizontal motion; however, this introduces a significant design limitation: the absence of guide rails or linear guides. Without a guiding mechanism, the base's movement may deviate from a true linear path, potentially leading to inaccurate test results or inconsistent loading on the cable. Another major drawback is the requirement for a relatively large linear actuator. Achieving the necessary 300 mm travel at a high speed demands a powerful actuator, which significantly increases the size and weight of the overall system. This conflicts with one of our primary design goals: to keep the test stand as compact and efficient as possible. The large actuator also influences the test fixture's footprint and potentially complicates the integration of other components.

Despite its limitations, this initial concept was highly valuable in shaping our understanding of the project's scope. It highlighted several critical areas for improvement, such as the need for precise guidance mechanisms for the moving base and more space-efficient actuation solutions. Going forward, many components from this design, such as the use of a linear actuator for controlled motion and the force sensor placement, will be retained and refined. The insights

gained from this concept will directly inform the next iterations of the test fixture, ensuring they are both functionally robust and aligned with the company's expectations for performance and form factor.

Design Iteration 2

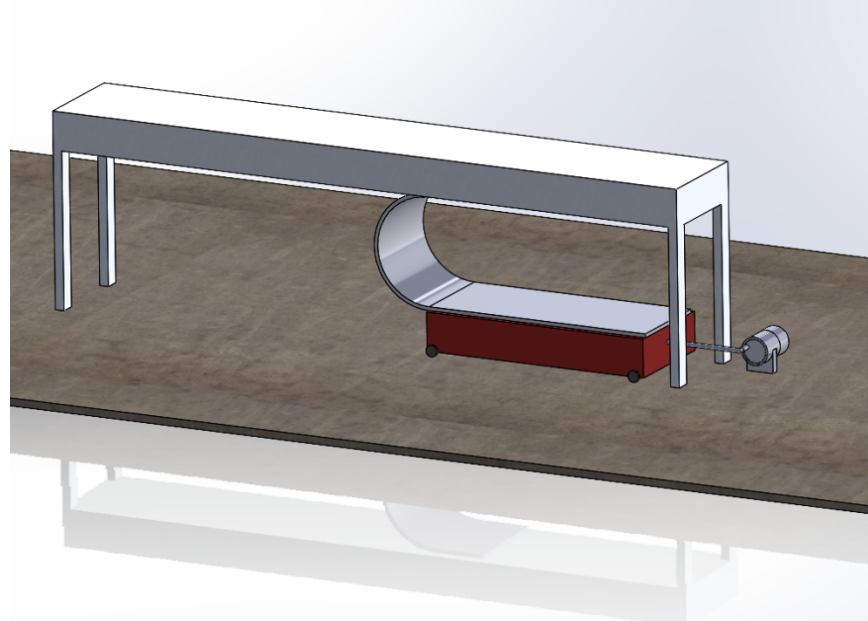


Figure 11 - Design Concept #2 for the Dynamic Test Fixture.

The design for this test setup aims to measure the force exerted by a cable on a fixed stand by coordinating several mechanical components. At the top, a fixed plate securely holds the upper end of the cable, establishing a stable anchor point. The bottom end of the cable is attached to a movable base mounted on wheels, allowing for horizontal movement. This base is actuated by a DC motor, which drives a connecting rod to convert rotational motion into linear motion. As the motor shaft rotates, the connecting rod pushes and pulls the base, simulating the dynamic motion experienced by cables in operational environments. A force sensor is strategically placed between the fixed stand and the cable to continuously capture the force exerted as the cable flexes and straightens during the test cycle. The cable is pre-bent, and as the movable base travels up to 300 mm, the cable undergoes significant bending, at times striking the sensor and fixed stand, creating the measurable force that the sensor records.

However, this design faces two significant drawbacks. First, the displacement of the base is inherently limited by the geometry of the motor shaft and the mechanics of the connecting rod. Given the motor shaft's radius of just 0.056 mm, each full rotation only generates 0.056 mm of linear movement at the base, an amount far too small to meet the 300 mm travel requirement. To overcome this, we considered attaching a large rotating disk to the motor, with the connecting rod mounted at the edge of the disk to amplify the motion. For 300 mm of displacement, a disk with a 150 mm radius would be required. While this modification increases the effective range of movement, it introduces new complications: the size of the disk could interfere with the fixed top plate, the connecting rod's swing path may create clearance issues, and the overall test stand footprint would increase significantly, contradicting our aim to keep the setup compact and manageable.

The second critical issue involves the stability of the movable base. Because the base is mounted on wheels without any guiding mechanism, there's a high risk of lateral swerving during operation. This side-to-side motion compromises the linearity of the displacement, introducing variability in the cable's loading and affecting the accuracy of the force measurements. Without guide rails or grooves to constrain the motion path, the system lacks the precision necessary for repeatable and reliable testing.

In summary, while this concept offers a creative mechanical solution using a DC motor and connecting rod to simulate dynamic motion, it is hindered by limitations in displacement capacity and motion accuracy. These challenges highlight the need for design refinements, such as implementing a more suitable actuation method and adding guidance systems to ensure true linear movement, both of which are essential for achieving the desired test performance.

Design Iteration 3

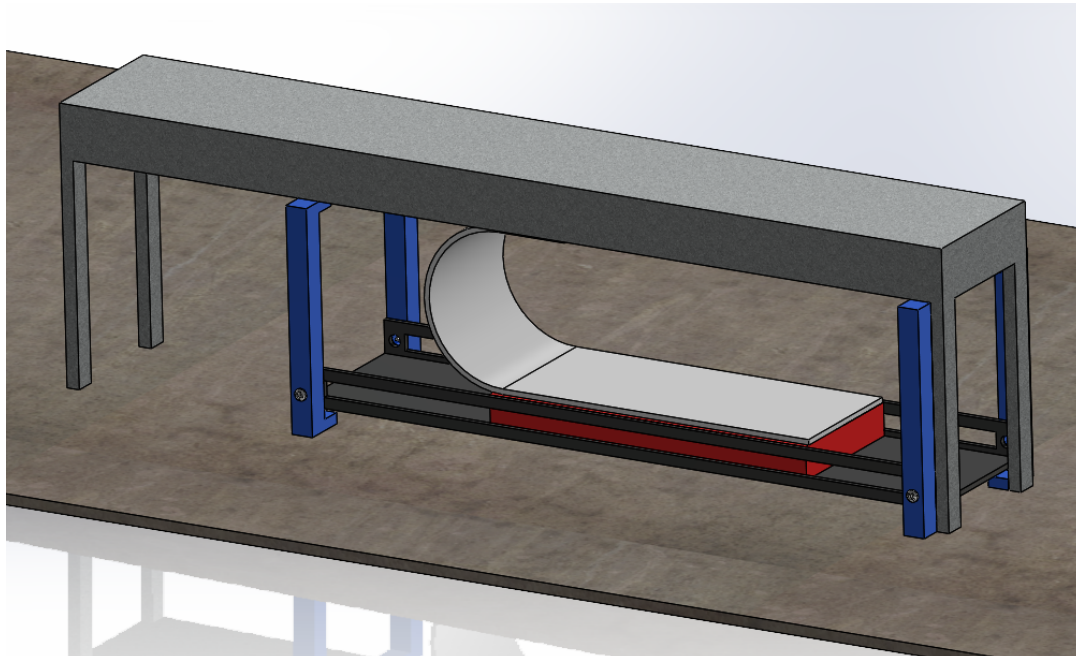


Figure 12 - Design Concept #3 for the Dynamic Test Fixture.

This revised design maintains the essential components of the previous setups, namely, the fixed top plate, movable base, cable, and force sensor, but introduces a new motion system centered around a stepper motor and a significantly redesigned movable base. Rather than relying on a connecting rod powered by a standard electric motor, the system now utilizes a stepper motor to deliver precise, incremental displacement. This provides significantly improved control over the motion profile, allowing for more accurate and repeatable cable testing. The movable base is no longer mounted on wheels; instead, it is built as a rectangular structure that slides along a pair of linear guide rails. These guide rails ensure strictly linear motion, eliminating the lateral swerving issues encountered in previous designs and significantly improving the consistency of the force measurement.

The platform supporting the movable base is elevated and rigidly fastened to the legs of the fixed table using screws, carefully preserving a vertical plate-to-plate spacing of 150 mm. This spacing is critical for maintaining the intended cable geometry during testing, ensuring that the

cable is bent consistently and that the force sensor readings reflect true mechanical behavior. Linear displacement is achieved through a modified actuator mechanism, consisting of a threaded rod coupled to the stepper motor. As the motor rotates, the nut traverses along the threaded shaft, converting the rotational input into linear motion. The rod itself is precisely 300 mm long, enabling the base to move across the entire required displacement range, which in turn induces the full bending profile in the 600 mm cable. This range is essential to replicate the extreme dynamic conditions that the cable would face in real-world applications.

However, this approach introduces some trade-offs. One of the main drawbacks is that the use of a threaded rod inherently limits speed and introduces less precise motion compared to other linear actuation methods. Threaded drives tend to have backlash and are generally slower due to the mechanical friction and the finer pitch required for controlled motion. Additionally, while the guide rails improve accuracy by constraining the motion path, they may also introduce unwanted friction, especially if not properly lubricated or aligned. This additional resistance could affect the responsiveness of the system and place extra load on the stepper motor, which must be accounted for during component selection.

Despite these limitations, the advantages of this design are substantial. The use of a stepper motor allows for fine-tuned displacement control, while the guide rails provide structural stability and motion linearity. The modular nature of the design also means that the size and length of the system can be modified to accommodate different cable types or test scenarios. Overall, this configuration addresses the major shortcomings of earlier concepts, particularly motion inaccuracy and instability, while offering a more scalable and precise testing solution.

Design Iteration 4

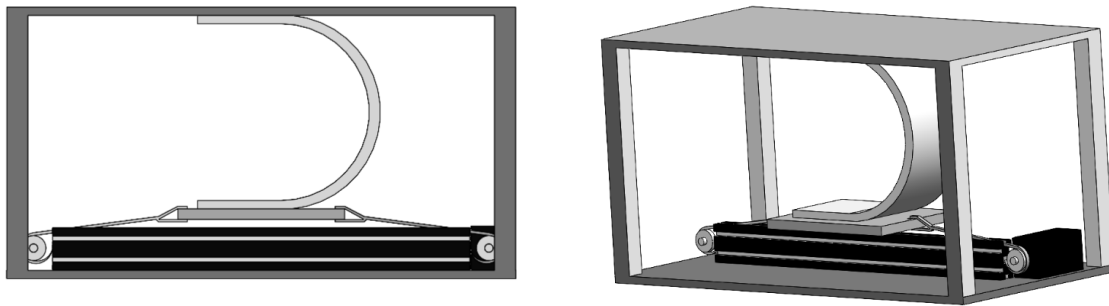


Figure 13 - Design Concept #4 for the Dynamic Test Fixture.

This design iteration builds upon the strengths of the previous concepts by introducing a belt-driven linear actuator housed within a box-type enclosure. It retains the use of the stepper motor from Design 3, leveraging its precise incremental control to manage displacement with high accuracy and repeatability. The belt-driven system provides a notable improvement in speed and smoothness of motion compared to the threaded rod used previously, allowing the movable base to traverse the full 300 mm range more efficiently. To maintain linearity and eliminate any lateral deviation during motion, the design incorporates a guide rail system, which ensures that the base moves in a straight and stable path. This setup directly addresses the key shortcomings of earlier designs, specifically, the motion instability caused by wheel-based platforms and the limited displacement capacity of connecting rod or threaded mechanisms.

Encasing the entire actuation assembly in a rigid, box-type structure adds structural integrity and protects the internal components from dust, debris, or mechanical interference, which is particularly important in precision testing environments. The belt mechanism also helps reduce friction and mechanical backlash, leading to smoother, quieter operation, an important factor when running repeated or high-speed test cycles. Furthermore, this design enables greater control over test parameters, including speed, acceleration, and positional accuracy, offering enhanced flexibility for various testing protocols. By integrating these elements, the design not only improves the reliability and consistency of force measurements but also provides a more refined and scalable platform for dynamic cable testing, aligning closely with the performance and precision requirements of the company's application.

Evaluation of Iterations

For this portion of our report, we will be evaluating every design mentioned in the previous section to determine the best design concept for our project. This evaluation works based on rating each design on some design attributes. These attributes are given a weight factor which is multiplied by the rating to obtain a score. The scores for each design attribute are totaled per design concept and compared at the end to determine the best design based on these attributes. The weight factors and ratings are chosen between 1 and 5, with 5 being the highest obtainable rating.

The attributes we will be considering for this project are as follows. We will also include a short description for each attribute to highlight what we feel are the important factors.

Design Attributes:

1. Speed of Operation:

For this attribute, we will be considering the speed at which we will be able to obtain our results. We will also consider the speed of the test as well, meaning that if a concept is working with a slower motor for the motion of the base, it will receive a lower rating.

2. Accuracy Achieved:

For this attribute, we will be considering the accuracy of the result output by the test stand. In our case, we will be basing this on the Force reading provided, and any potential errors which may occur during our measurements.

3. Reliability:

For this attribute, we will be considering the overall consistency of the design concept. We want our test stand to repeatedly perform in the same way under the same conditions. In addition to this, we will also consider any possible malfunctions in the design.

4. Durability:

For this attribute, we will be considering the durability of the design concept. This means that we will consider the potential failure points of each design and base our rating on this.

5. Environmental Robustness:

For this attribute, we will be considering the overall robustness or strength of our design. We want our test stand to be able to work in almost any environment but acknowledge that this might be difficult especially since we are using many moving components which can degrade when used in certain environments. An example would be the usage of guide rails in dusty environments which can cause irregularities in the movement of a component.

6. Size and Weight:

For this attribute, we will be considering the overall footprint of the test stand. In our case the weight of the stand would be relatively similar across all of our designs, thus we will be focusing on rating our designs based on their compactness.

7. Prime Power Needed:

For this attribute, we will be considering the amount of power required to run our tests. The major components requiring power are the motors or actuators moving the base.

8. Installation Complexity:

For this attribute, we will be considering the effort required to set up the test stand and start acquiring results. All of our designs require the cable to be added manually, but some need additional setup in the case of an adjustable plate-to-plate distance.

9. Operation & Safety:

For this attribute, we will be considering the overall safety of the design. For this project, the idea is to encase every design with either clear acrylic or plastic to ensure safety. Thus, we can expect similar ratings for all designs for this attribute.

10. Maintenance & Service:

For this attribute, we will be considering the amount of maintenance required to keep the design running smoothly. We will consider designs with more moving components to require more maintenance, as these are more prone to failure.

11. Environmental Impact:

For this attribute, we will be considering the negative impact each design has on the environment. In our case all of our designs are pretty similar in that regard, all only run on electricity resulting in minimal pollution compared to an engine running on gasoline.

12. Testability:

For this attribute, we will be considering the effectiveness of each design to be tested for any issues or faults. In this case, as our designs are similar to each other, we will be taking into account the number of components that need to be tested for any faults/issues.

13. Life Cycle Costs:

For this attribute, we will be considering the overall cost to build and maintain each design. In our case, we can expect to focus on the initial costs of purchasing the motors or actuators and any other main components.

14. Human Factors & Appearance:

For this attribute, we will be considering the overall look of the design. As this is subjective to everyone we decided to focus on the size/overall footprint of each design. We are keeping in mind that every design will be encased in clear acrylic or plastic and will consider this in our ratings.

15. Manufacturability:

For this last attribute, we will be considering the manufacturability of each design. We will keep in mind the complexity and the amount of work required to assemble each design.

Design Attributes	Weight Factor	DESIGN 1		DESIGN 2		DESIGN 3		DESIGN 4	
		RATING	SCORE	RATING	SCORE	RATING	SCORE	RATING	SCORE
Speed of Operation	5	2	10	4	20	4	20	5	25
Accuracy Achieved	5	3	15	3	15	4	20	5	25
Reliability	5	3	15	3	15	3	15	4	20
Durability	3	4	12	4	12	3	9	4	12
Environmental Robustness	3	4	12	4	12	4	12	4	12
Size and Weight	4	2	8	2	8	5	20	5	20
Prime Power Needed	2	3	6	3	6	3	6	5	10
Installation Complexity	4	3	12	3	12	3	12	3	12
Operation & Safety	3	3	9	2	6	3	9	5	15
Maintenance & Service	2	4	8	4	8	3	6	3	6
Environmental Impact	2	4	8	4	8	4	8	4	8
Testability	1	4	4	4	4	4	4	4	4
Life Cycle Costs	5	2	10	4	20	3	15	3	15
Human Factors & Appearance	3	3	9	3	9	4	12	5	15
Manufacturability	3	4	12	4	12	3	9	3	9
Total Score			150		167		177		208

Table 1: Evaluation of Concepts using specific Design Attributes

Final Design Choice

Having thoroughly analyzed and discussed each design iteration and its key attributes, we are now in a position to evaluate and rank the concepts based on a set of defined performance criteria. After scoring each design against parameters such as accuracy, reliability, speed, manufacturability, and overall feasibility, Design 4 emerged as the most effective solution, achieving a total score of 208. This places it 31 points ahead of the next closest competitor, Design 3, indicating a clear performance advantage.

Design 4 excelled particularly in the categories of Speed of Operation, Accuracy, and Compactness, factors that are critical to our test setup's intended functionality and integration within the broader system environment. The use of a belt-driven linear actuator and a stepper motor provided smoother and faster motion compared to previous designs, while the inclusion of guide rails ensured consistent linear displacement with minimal deviation. Additionally, the enclosed box-type structure contributed to a more refined, space-efficient footprint, which is essential for test environments with limited space and high cleanliness standards.

In terms of Reliability, Durability, Testability, and Manufacturability, Design 4 performed consistently well, matching or slightly exceeding the other concepts. Its modular layout and enclosed components contribute to easier maintenance and protection from environmental factors, enhancing long-term reliability. Furthermore, its straightforward mechanical assembly and standardized components improve manufacturability and reduce potential issues during production or testing. Overall, Design 4 represents a well-balanced solution that successfully addresses the shortcomings of previous iterations while meeting the company's operational and engineering standards.

Analysis of Design

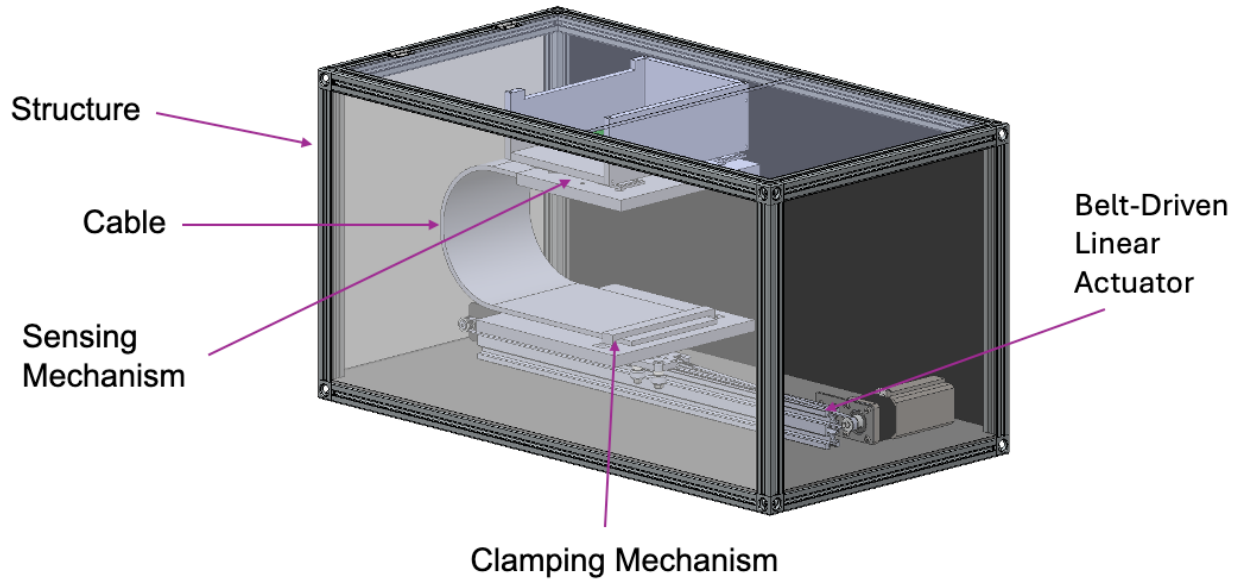


Figure 14 - Final Design CAD model.

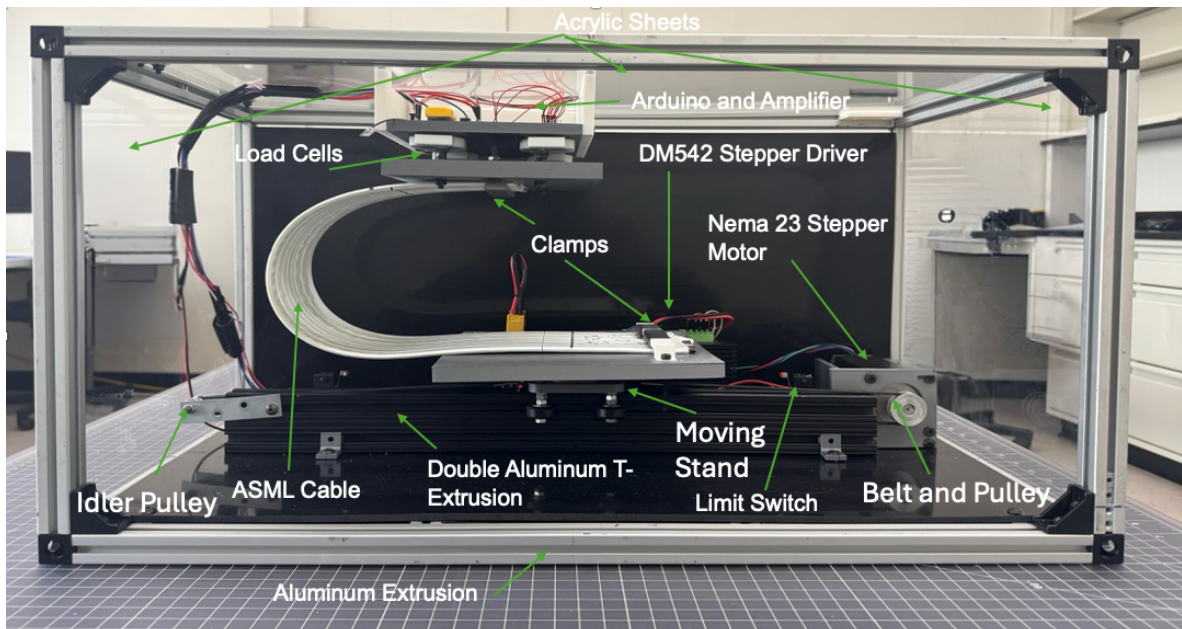


Figure 15 - Final Design Front View.

Here we can see the final manufactured dynamic test fixture in its fully assembled state. This front view introduces the complete system and offers a clear look at the integration of all major mechanical and electrical components. The test fixture is built around a rigid aluminum extrusion frame and enclosed with a combination of HDPE and clear acrylic panels for protection and accessibility. Inside the enclosure, the ASML cable is mounted between two clamping platforms — one fixed at the top and the other attached to the moving stand, which is driven by a belt and pulley system connected to a NEMA 23 stepper motor. A double aluminum T-extrusion serves as the base for the actuator and guide rail system, enabling smooth and controlled motion. Load cells mounted at the top capture the force exerted by the cable, while an HX711 amplifier

and Arduino Giga R1 handle data acquisition and system control. All components are strategically arranged to maintain a compact footprint while meeting the functional requirements of precise force measurement and repeatable motion cycles.

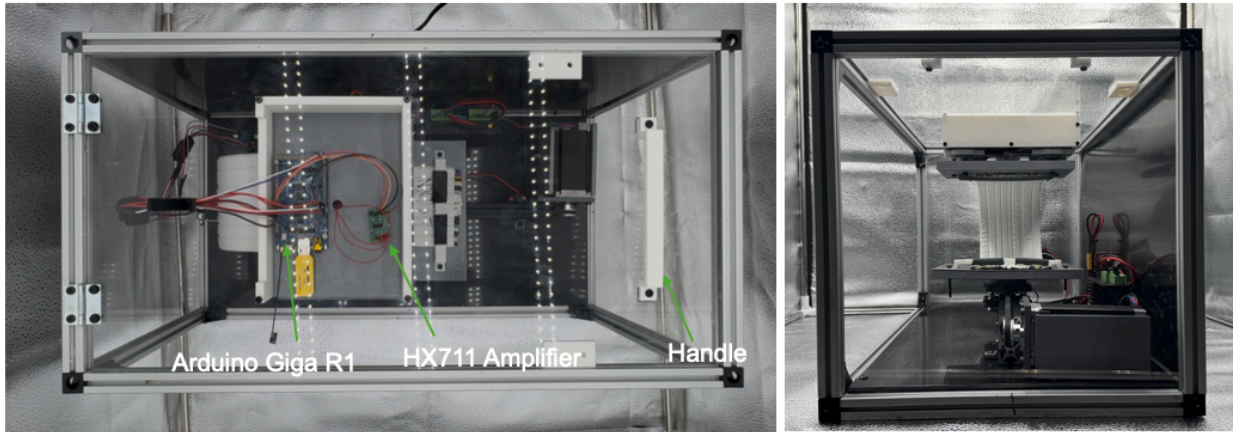


Figure 16 - Final Design Top (left) and Side (right) View.

These views show the test fixture from the top and side. Key electrical components are visible from the top, including the Arduino Giga R1 and HX711 amplifier, while the side view highlights the vertical structure and internal arrangement.

Structure

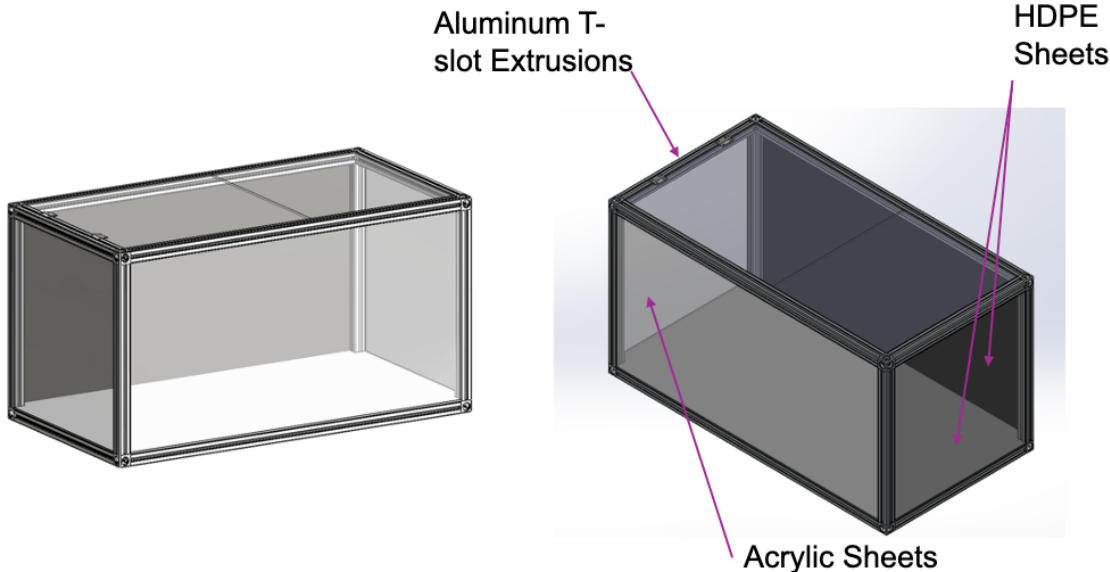


Figure 17 - CAD Model of Final Design Structure.

The structural subassembly consists of aluminum extrusion profiles that form the primary frame of the test fixture, providing strength, rigidity, and modularity. High-density polyethylene (HDPE) plates are installed along the back and bottom surfaces to provide visual contrast for observation and improved background uniformity during testing. Clear acrylic sheets are mounted on the top and sides of the structure to allow visibility of internal components while serving as protective barriers to ensure user safety during motion cycles. The front of the fixture remains open to facilitate easy access for cable installation, adjustment, and maintenance.

Belt-Driven Linear Actuator

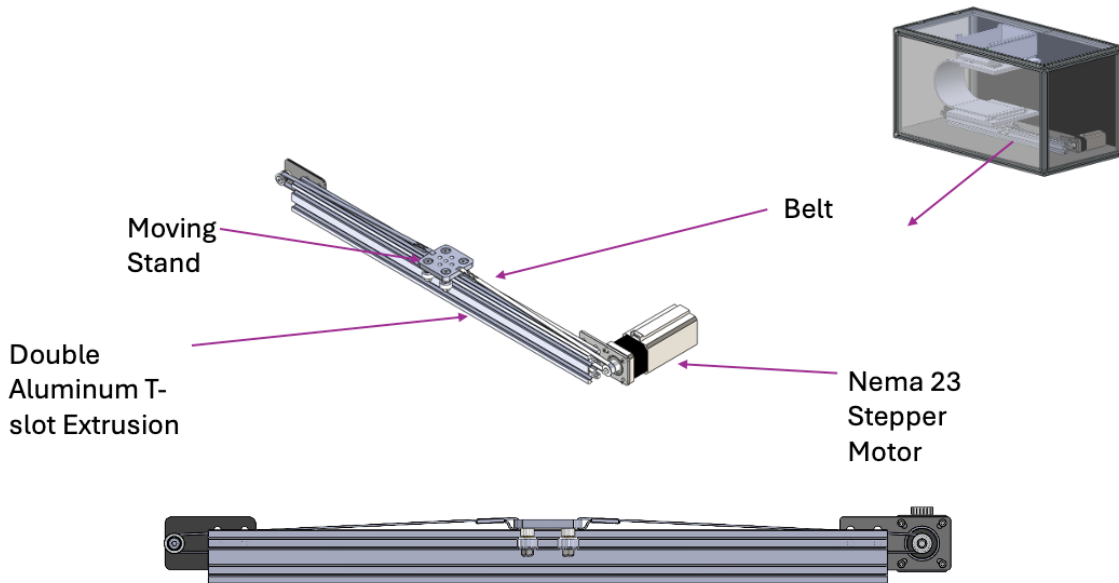


Figure 18 - CAD Model of Belt-Driven Linear Actuator.

The belt-driven linear actuator serves as the main motion mechanism in the test fixture, enabling precise horizontal displacement. It features a closed-loop timing belt driven by a stepper motor and tensioned around pulleys at both ends. Attached to the belt is the moving stand, which holds the lower cable clamp and travels smoothly along the linear path. The entire assembly is mounted onto a double aluminum extrusion, which integrates both the belt track and guide rail system into one structural unit. This configuration ensures compactness, high-speed motion, and reliable alignment over the full 300 mm travel range.

Sensing Mechanism

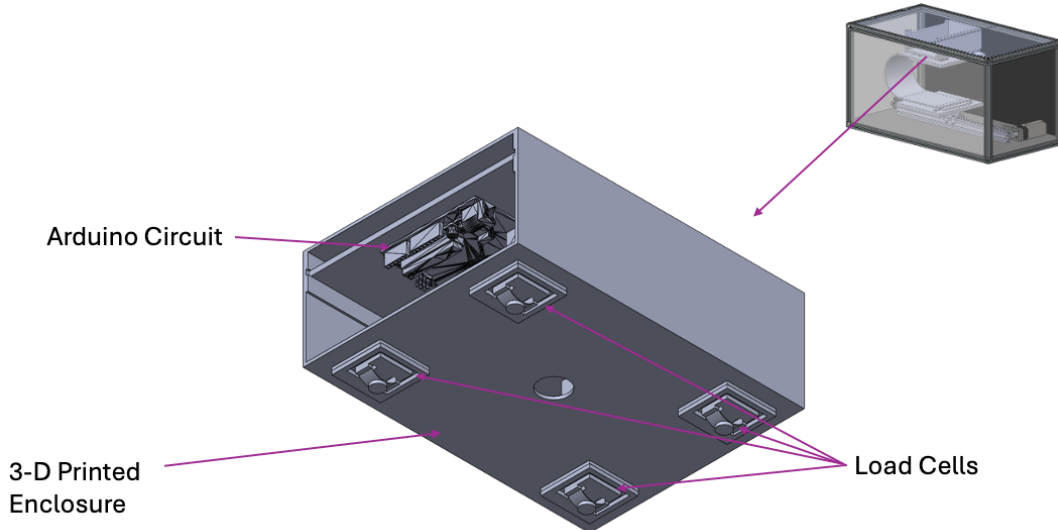


Figure 19 - CAD Model of Final Design Sensing Mechanism.

The sensing mechanism includes a load cell mounted on the top plate to detect the force applied by the cable. An HX711 amplifier interfaces the load cell with an Arduino microcontroller,

which handles both data acquisition and full system control, including motor operation and calibration routines. All components are enclosed within protective housing to ensure organization, safety, and ease of access during testing and troubleshooting.

Clamping Mechanism

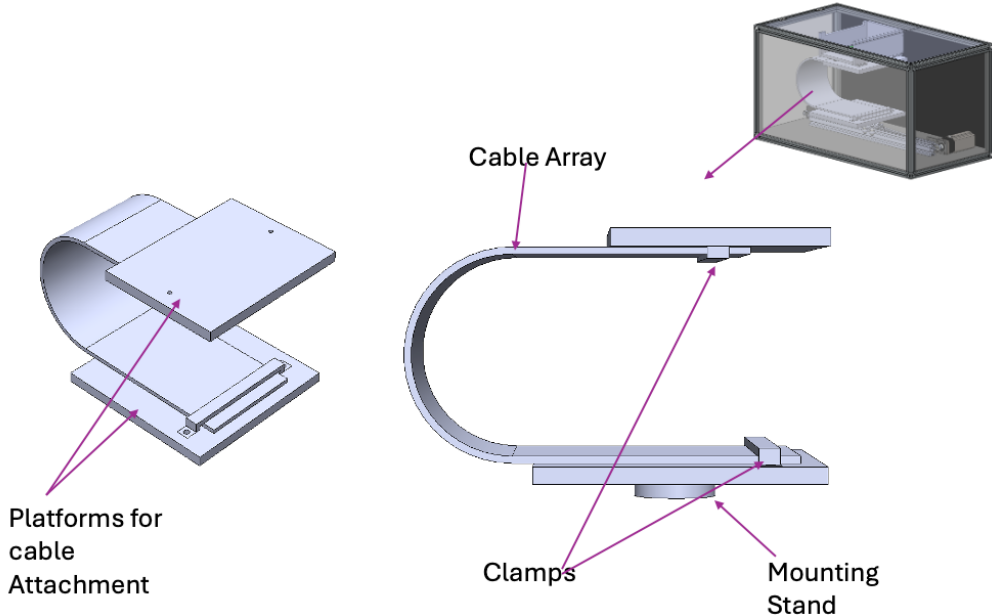


Figure 20 - CAD Model of Final Design Clamping Mechanism.

The clamping mechanism consists of custom clamps mounted onto dedicated platforms that serve as attachment points for the cable ends. One platform is fixed at the top of the structure, while the other is mounted on a stand secured to the moving base of the belt-driven linear actuator. These platforms ensure proper alignment and spacing of the cable while the clamps maintain a secure grip during motion. This configuration supports the required fixed-fixed boundary condition necessary for consistent and accurate testing.

Test Fixture Without Enclosure

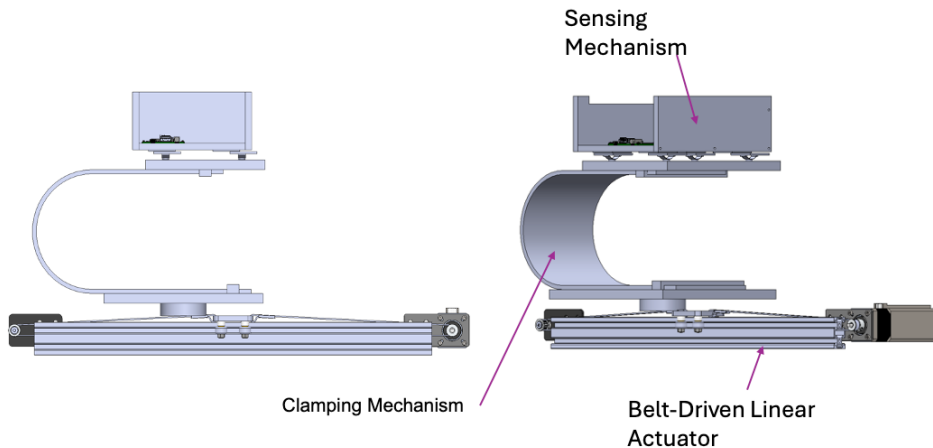


Figure 21 - CAD Model of Final Design without Enclosure.

Here we can see the test fixture without the enclosure. Visible components include the clamping mechanism, the belt-driven linear actuator, and the sensing mechanism.

System Circuit Diagrams and Wiring Configuration

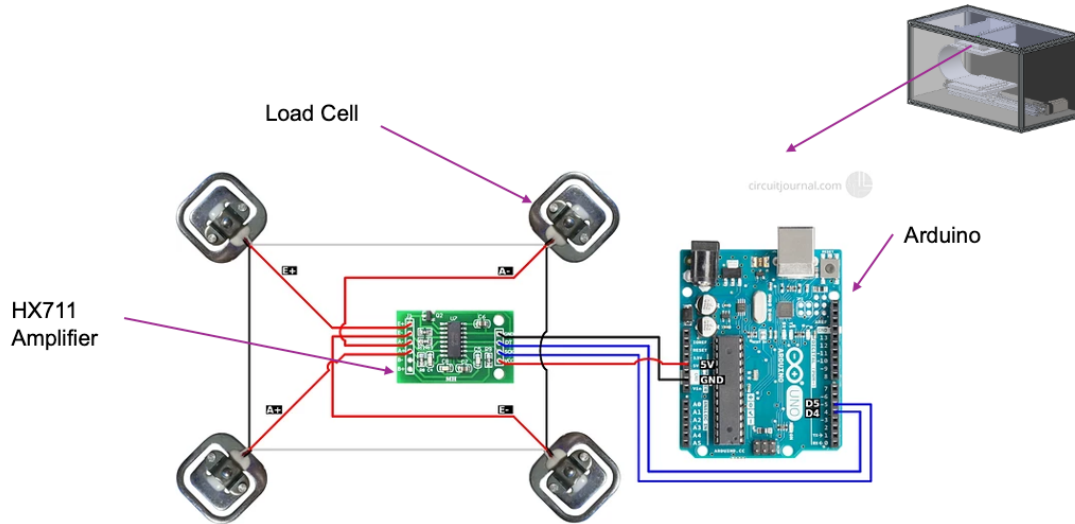


Figure 22 - Load Cell and Amplifier Circuit

Figure 20 above shows the circuit used to read force data from the load cells. Four load cells are connected in a full Wheatstone bridge configuration and interfaced with an HX711 amplifier module. The amplifier converts the analog signal from the load cells into a digital signal, which is sent to the Arduino for processing. This setup allows accurate force measurements to be collected during testing. The layout demonstrates how the load cells are wired to the amplifier and how the amplifier connects to the Arduino.

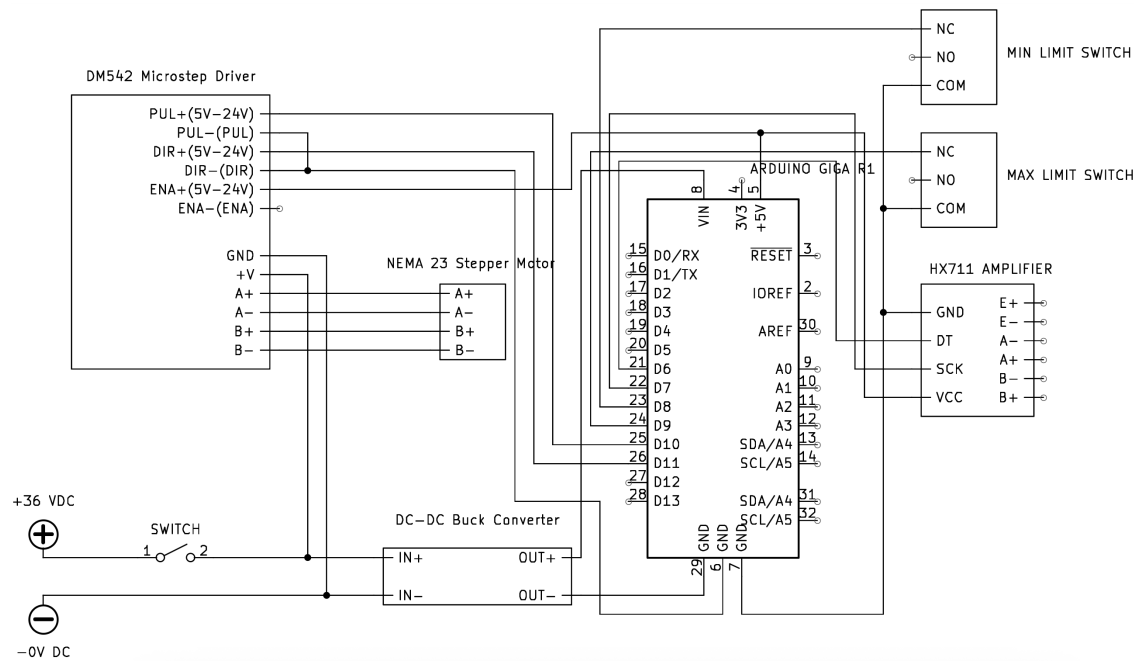


Figure 23 - Wiring Diagram for Full System.

Figure 21 above presents the full wiring diagram for the dynamic test fixture, showing how all electrical components are connected. Power enters the system through a 36V DC supply and passes through a switch, where it is split into a parallel connection. One branch delivers 36V directly to the DM542 stepper driver to power the NEMA 23 stepper motor. The second branch routes 36V to a buck converter, which steps the voltage down to 5V to power the Arduino Giga R1 and the HX711 amplifier. The Arduino serves as the central controller, coordinating motion control via the stepper driver and data acquisition from the load cell through the amplifier. Limit switches are included to provide safety and calibration references for motor travel. This diagram captures the full integration of the motion, sensing, and power systems.

System Operation Breakdown

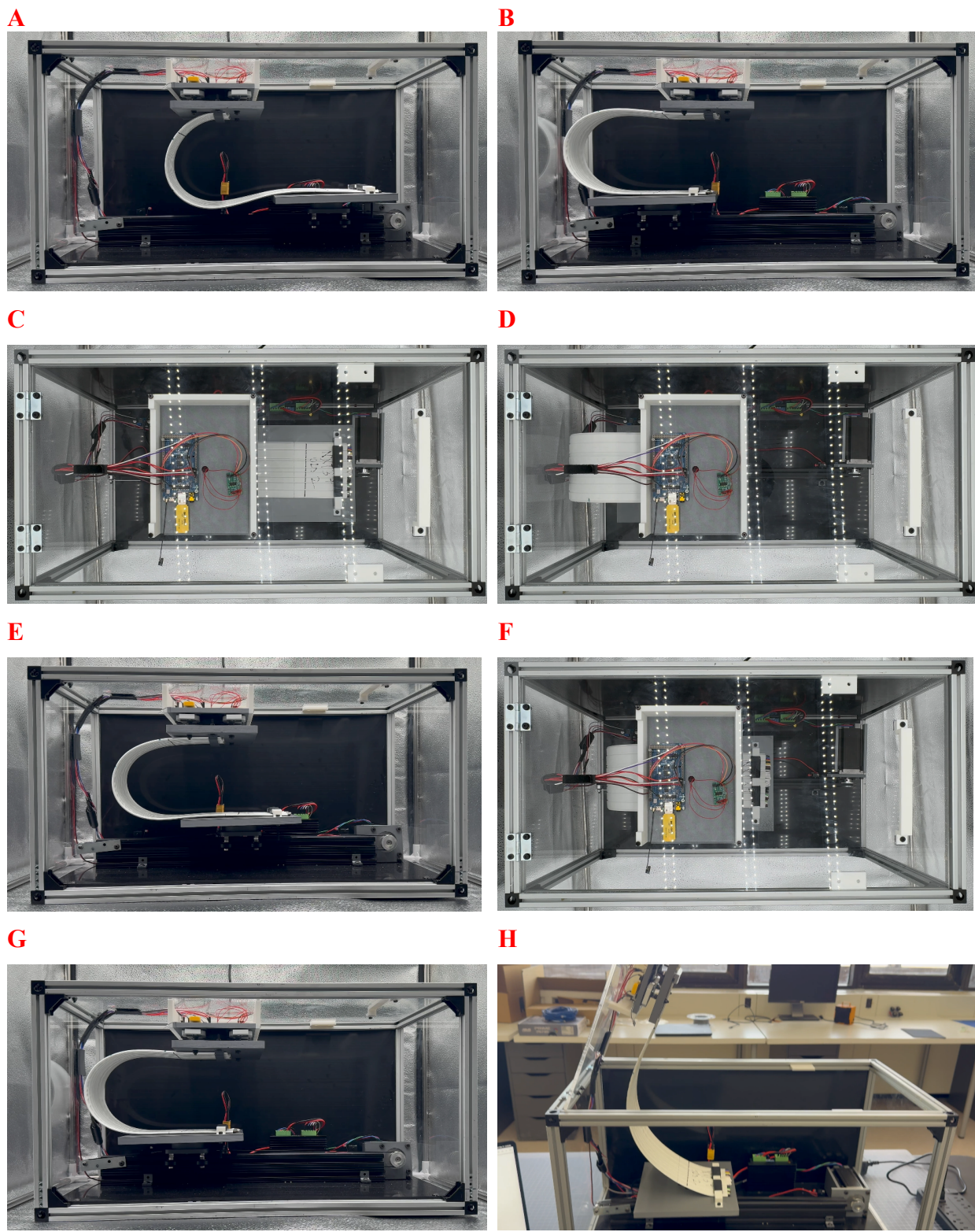


Figure 24 – Step-by-Step System Operation.

The operation of the dynamic test fixture is controlled through a custom web-based interface hosted on the Arduino, shown in Figure 25. The interface includes buttons to initiate calibration, run motion loops, stop and return to center, move to a specific position in millimeters, and export the collected data.

To begin, the user selects “Start Calibration”, which initiates a sequence to determine the full travel range of the system. Upon starting calibration, the stepper motor rotates clockwise until it triggers the minimum limit switch, as shown in Figure 24A. It then reverses direction and moves counterclockwise until it reaches the maximum limit switch, as seen in Figure 24B. These steps are also captured from the top view in Figures 24C and 24D, respectively.

This calibration process allows the system to determine the total number of steps between the two mechanical limits. From this, the software calculates the center position, which is used as a reference for all subsequent motion commands. Once the center is determined, the motor automatically moves to that location, as shown in Figures 24E and 24F. At this point, the system is calibrated and ready for operation.

After calibration, the user can select a loop command (e.g., Loop 1, Loop 5, Loop 10) from the website. These commands cause the system to oscillate back and forth between two defined edge positions, calculated to represent 90% of the total travel distance. This safety margin ensures the system never reaches the physical limit switches during normal operation. In addition to this, limit switch safety logic is implemented in the code: if either limit switch is triggered during normal operation (outside calibration), the system will immediately stop and return to the center to prevent mechanical damage.

The system defines the 0 mm reference point as the position where the two clamps are vertically aligned, as shown in Figure 24G. Positions to the right of this reference are treated as positive, and those to the left are negative. This convention allows the software to convert between step counts and physical displacement in millimeters using the known distance between limit switches.

The web interface also includes a manual control feature that allows the user to move the platform to any desired position by entering a value in millimeters. In this case, the platform was moved to the position shown in Figure 24G to create enough slack in the cable, allowing the top plate to be opened as shown in Figure 24H. This access is useful for installing the cable and performing any required adjustments or maintenance.

Once a loop has been completed, the user can export the recorded data by selecting the “Export Log” button. The system saves the timestamped position and force data to a connected USB flash drive, which is then used for further analysis and calculations.

Stepper Logger Control

Start Calibration

Loop 1 **Loop 3** **Loop 5** **Loop 10**

Stop and Return to Center

Export Log

Enter mm **Move to mm**

Figure 25 - Website Control Interface

Results

Results of Finite Element Analysis

Figure 26 depicts the stress distribution and displacement. According to this data, the maximum displacement was 2.176mm and the maximum Von-Mises stress was 27.84MPa. This confirms our theory that the simulation will have smaller results for these values since the model contained a solid structure rather than stranding.

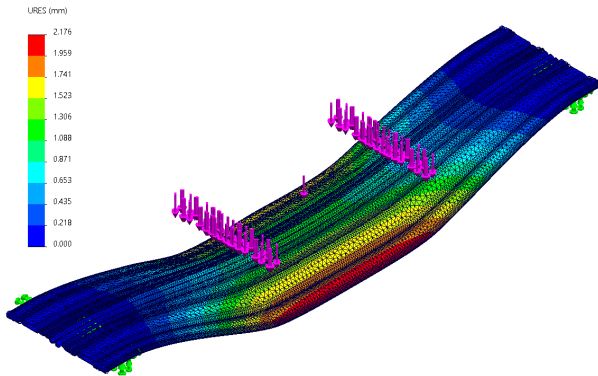


Figure 26 - Displacement distribution and constraints for the simulated four-point bend test.

Furthermore, the cable did not experience linear bending due to the asymmetrical layout of the wires. This can be seen in Figure 27, where the sides deform more than the center. As a result, the value for maximum displacement is not an accurate representation of the strain experienced by the cable due to the load. A better alternative is to replace the load with a predetermined displacement in the simulation and determine the stress from there. However, the simulation software ran into many issues, so we used the average displacement from the first study instead.

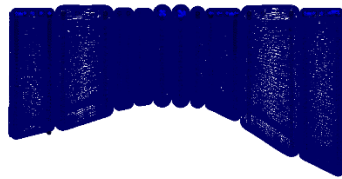


Figure 27 - Curvature of the cable array due to the loading as seen from the front.

Results of Four-Point Bend Test

Trial 1

Test #	Mass (g)	Force (N)	Displacement (mm)	Stress (Pa)	Strain	Bending Modulus (MPa)
1	212.4	2.083644	5.21	305221.2891	0.00073966	412.6492236
2	270.9	2.657529	6.75	389286.4746	0.0009583	406.2276453
3	301.7	2.959677	7.18	433546.4355	0.00101934	425.3193183
4	332.5	3.261825	8.55	477806.3965	0.00121384	393.6314392
5	364.8	3.578688	8.82	524221.875	0.00125217	418.6494141
6	397	3.89457	9.48	570493.6523	0.00134587	423.8834033
7	424.3	4.162383	10.16	609724.0723	0.00144241	422.7110171
				Average		414.7244944

Table 2 - Summary of Four-Point Bend Test Results (Data Set 1).

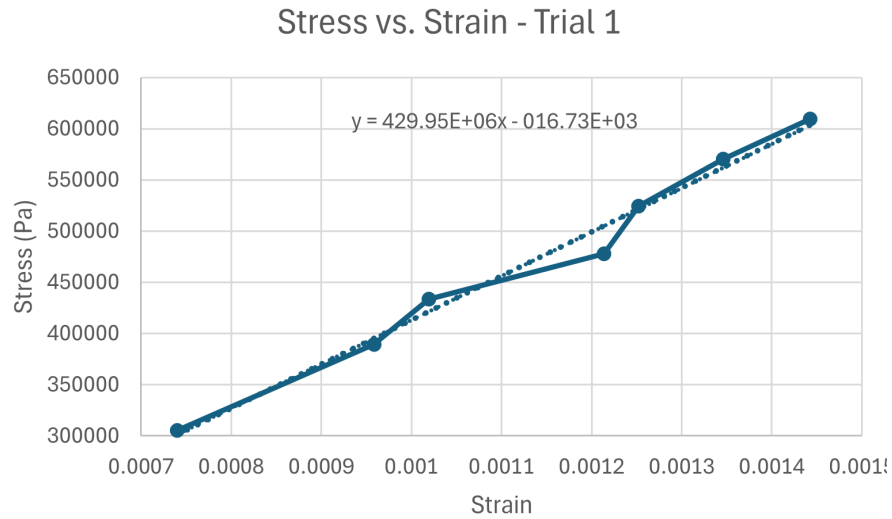


Figure 28 - Stress-Strain Analysis for Data Set 1.

Trial 2

Test #	Mass (g)	Force (N)	Displacement (mm)	Stress (Pa)	Strain	Bending Modulus (MPa)
1	212.4	2.083644	5.57	305221.2891	0.00079077	385.9788967
2	270.9	2.657529	6.85	389286.4746	0.00097249	400.2973147
3	301.7	2.959677	7.75	433546.4355	0.00110027	394.0377684
4	332.5	3.261825	8.2	477806.3965	0.00116415	410.4327811
5	364.8	3.578688	8.98	524221.875	0.00127489	411.1901817
6	397	3.89457	10.11	570493.6523	0.00143531	397.469304
7	424.3	4.162383	10.44	609724.0723	0.00148217	411.37394
				Average		401.5400267

Table 3 - Summary of Four-Point Bend Test Results (Data Set 2).

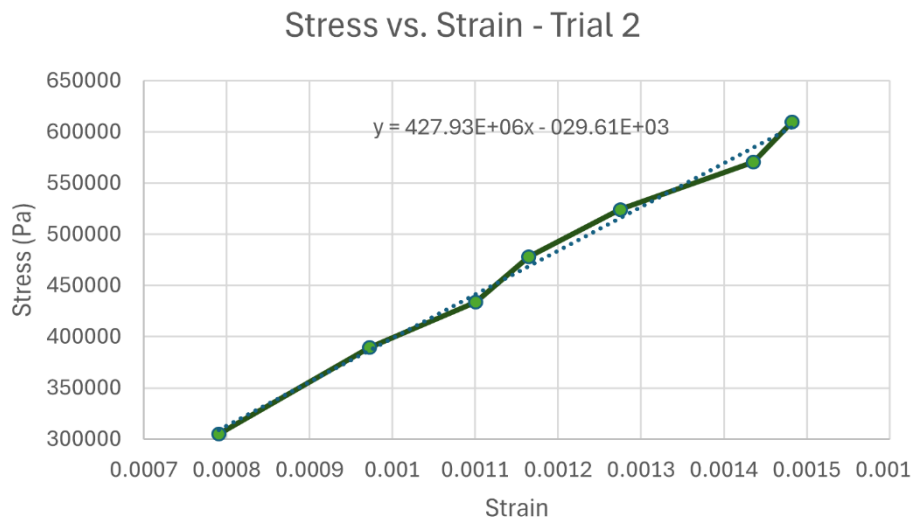


Figure 29 - Stress-Strain Analysis for Data Set 2

From these 2 trials, we were able to obtain the following for the Bending Modulus:

Trial	Bending Modulus (MPa)
1	429.95
2	427.93
Average	428.94

Table 4: Results for 4-point Static Analysis

Using this average value for the Bending Modulus, we are able to approximate the Bending Stiffness by multiplying it by the 2nd Moment of Inertia. The only issue with this is that the cable has an extremely complicated cross-section, meaning that we will have to approximate it as a rectangle. When doing this, we obtain an Approximate Moment of Inertia (I):

$$I = 608 \text{ mm}^4$$

Now we can use the value to obtain the Bending Stiffness (EI):

$$EI = 428.94 \text{ N/mm}^2 \cdot 608 \text{ mm}^4 = 2.605 \times 10^5 \text{ Nmm}^2$$

This value will be used to compare our results using the different methods (Static & Dynamic).

Results of the Dynamic Test

Using our test fixture, we were able to obtain an approximate value for the Bending Stiffness of the ASML cable. We ran 5 different tests and obtained the Bending Stiffness for each one, from which we took the average to obtain our final result. In the following graphs, you will find the results for the Bending Stiffness versus Time. Also important to note is that for our follow-up calculations based on the data in these graphs, we have decided not to use every single Bending Stiffness data point to obtain the average result. This is because the cable was observed to be sagging when it reached the extremes of the travel distance. From this observation, we decided to exclude datapoints after a certain position (190mm). Another observation we made after obtaining the data was that there are points in time when the cable crosses the zero position during the loops. Because of the way our final equation for the Bending Stiffness is set up, we were getting extremely high peaks of datapoints for the Bending Stiffness. To combat this, we decided to exclude any data where the cable would go past the zero position in the negative direction and only decided to observe the positive region ($x > 0.5\text{mm}$).

Trial 1

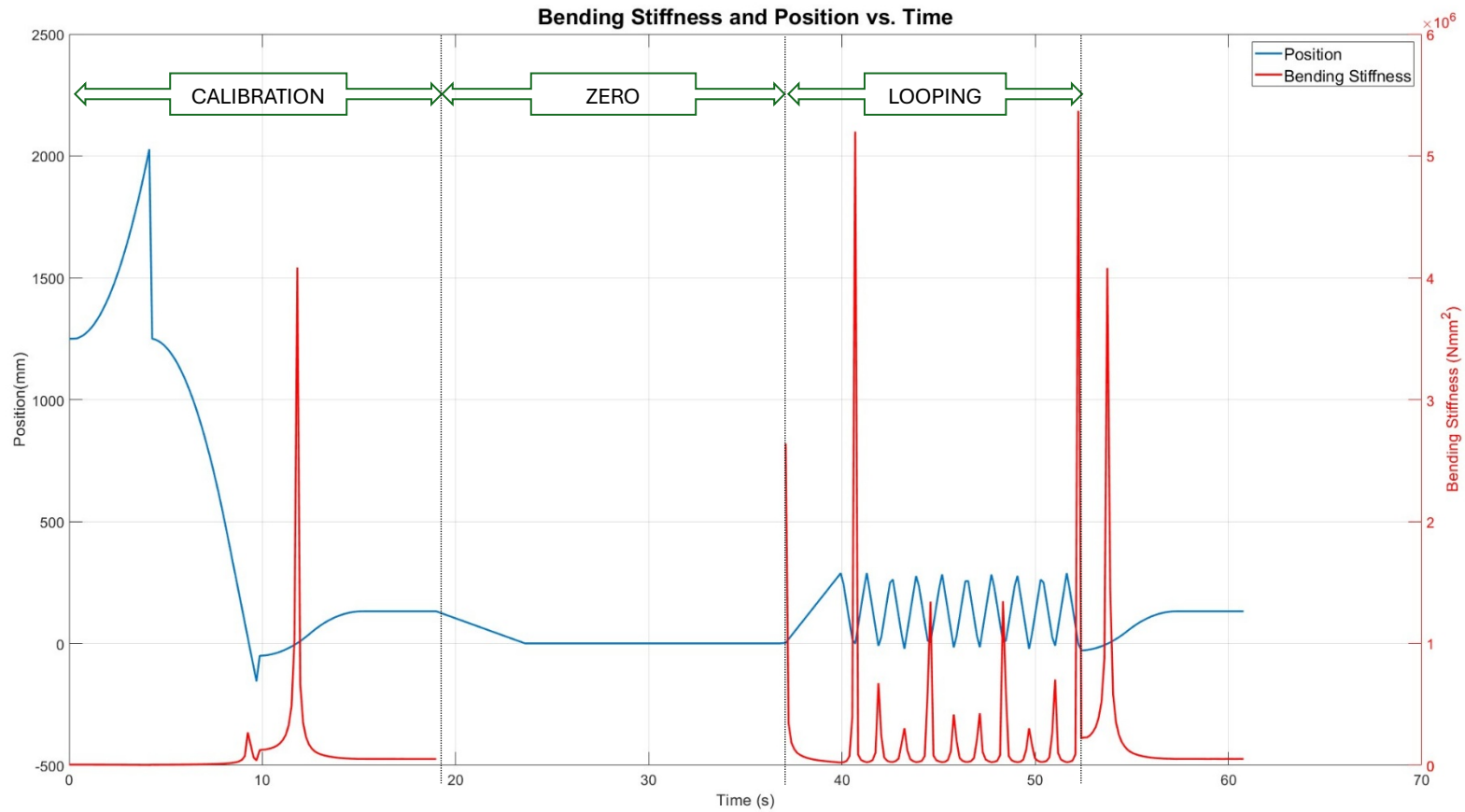


Figure 30 - Bending Stiffness and Position vs. Time for Trial 1 of the Dynamic Analysis.

Trial 2

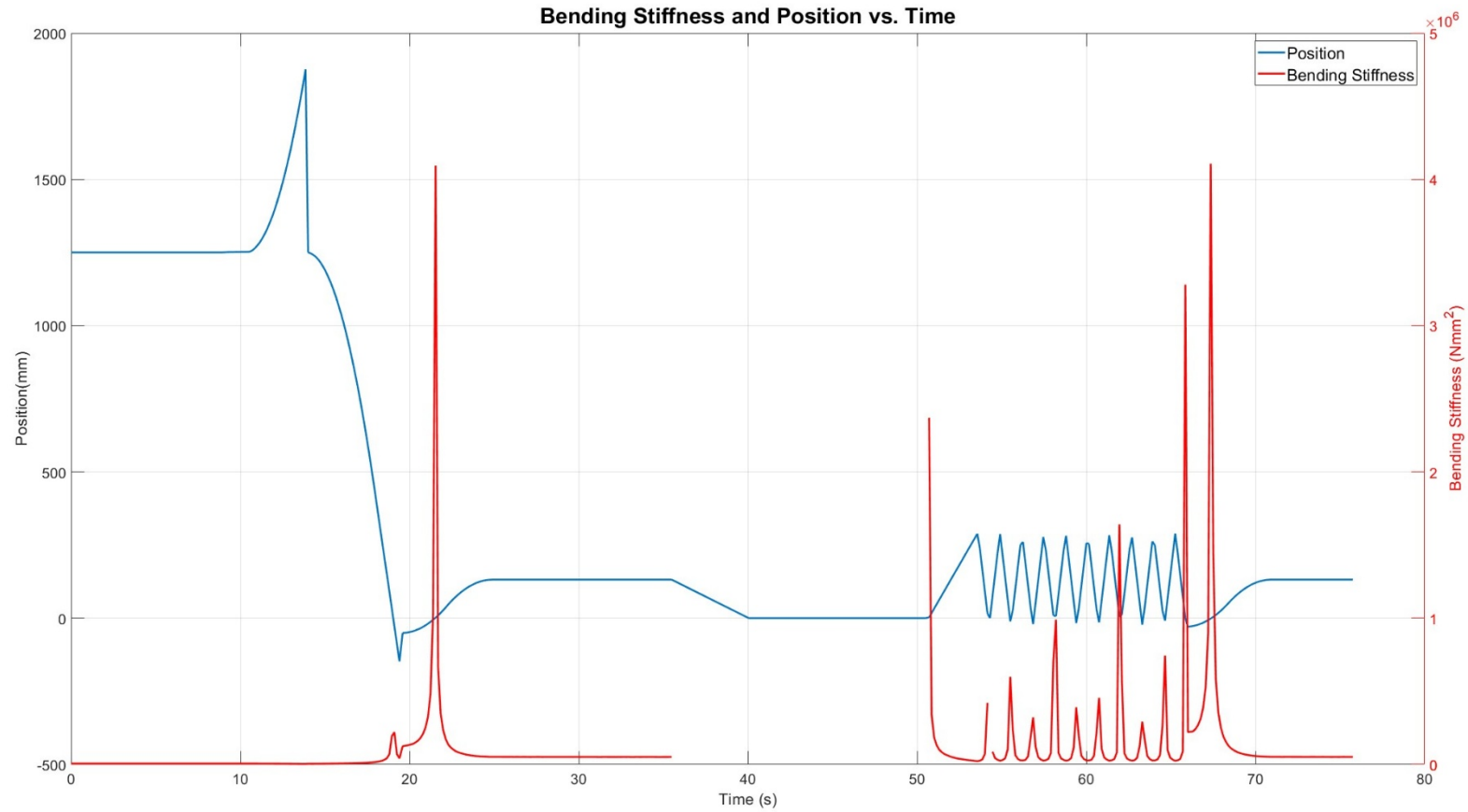


Figure 31 - Bending Stiffness and Position vs. Time for Trial 2 of the Dynamic Analysis.

Trial 3

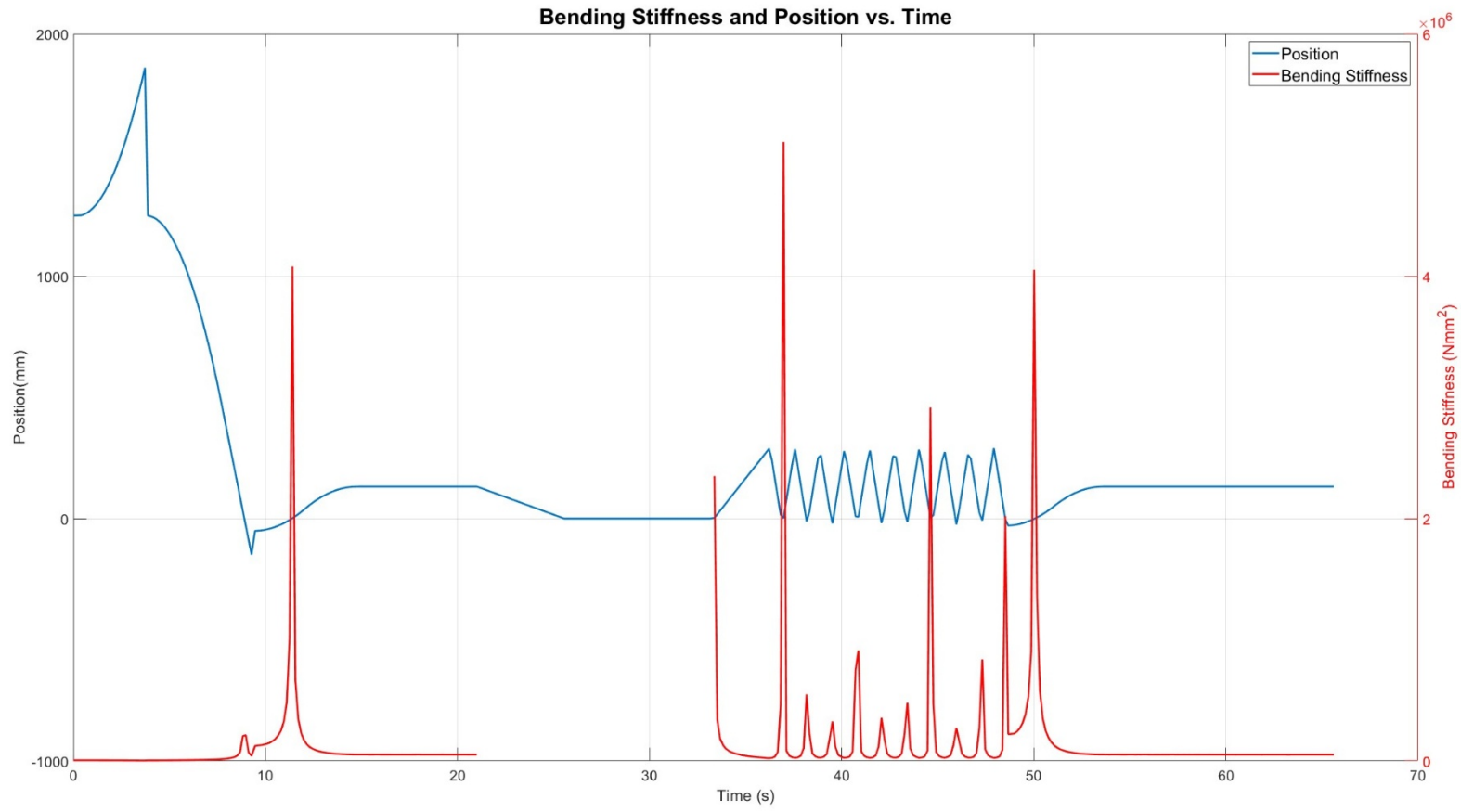


Figure 32 - Bending Stiffness and Position vs. Time for Trial 3 of the Dynamic Analysis.

Trial 4

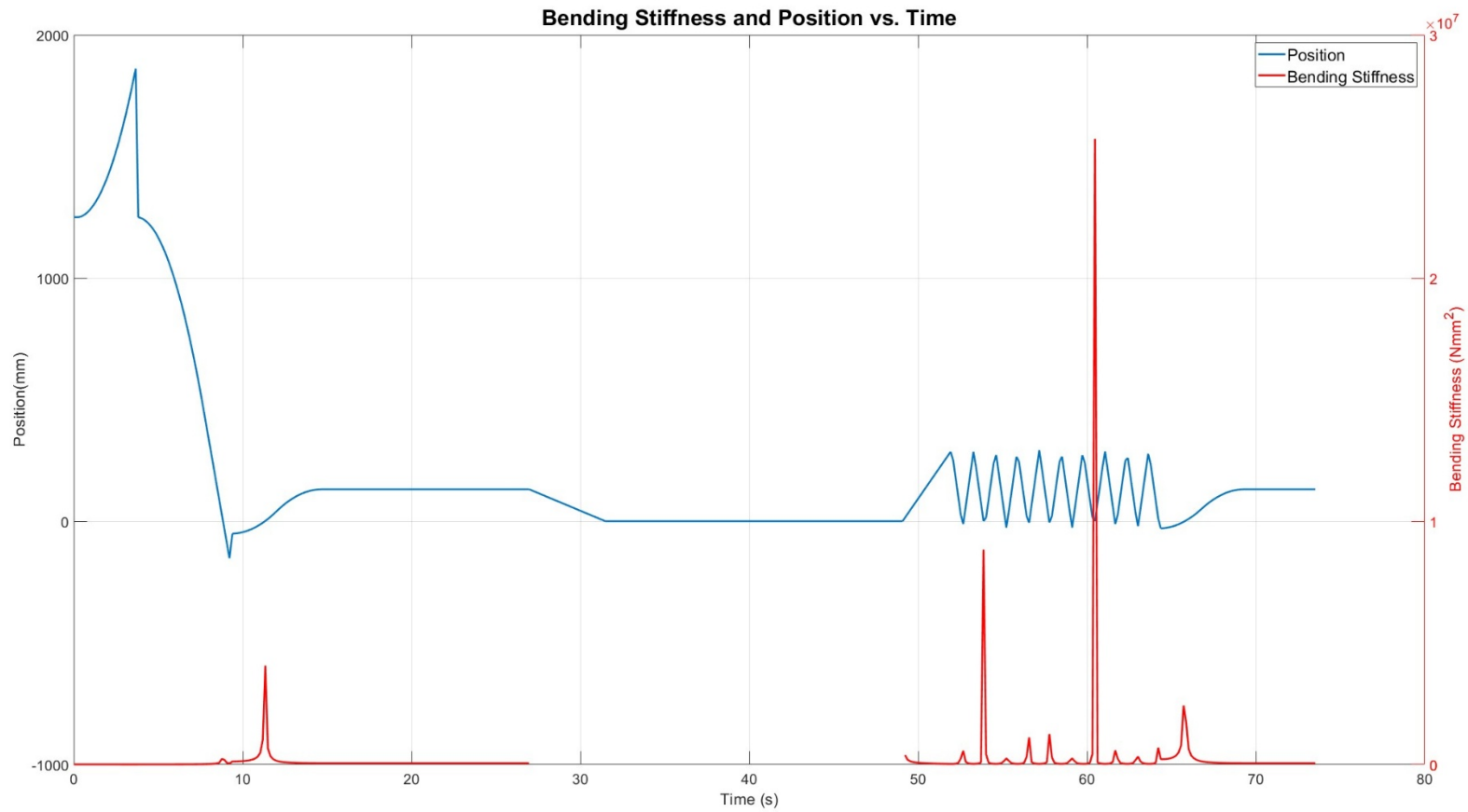


Figure 33 - Bending Stiffness and Position vs. Time for Trial 4 of the Dynamic Analysis.

Trial 5

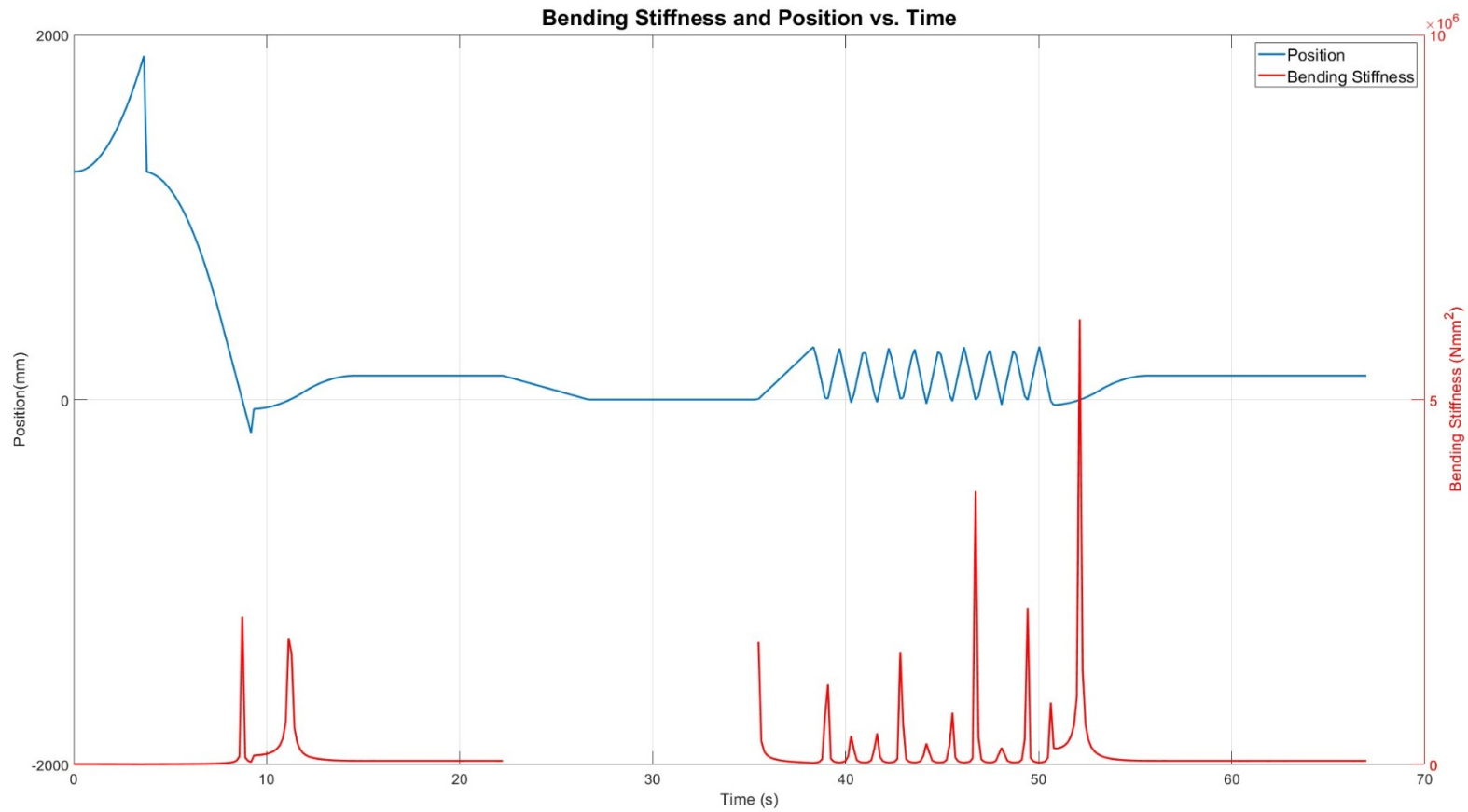


Figure 34 - Bending Stiffness and Position vs. Time for Trial 5 of the Dynamic Analysis.

After gathering all the relevant data points for the Bending Stiffness from each trial we are now able to calculate the average result.

Trial	Mean Bending Stiffness (Nmm ²)
1	1.657×10^5
2	1.307×10^5
3	1.533×10^5
4	1.536×10^5
5	1.062×10^5
Average	1.419×10^5

Table 5: Results for Dynamic Analysis.

Discussion of Results

The four-point bend test was a critical step in understanding the mechanical behavior of the cable arrays. By conducting two separate trials, each with multiple data sets, we ensured that variability in the results was minimized and that the measurements were reliable. Utilizing Equations 1 and 2 to find the bending stress and strain at each applied load, we were able to transform the values into a bending modulus with Equation 3. Trial 1 produced a bending modulus of 429.95 MPa, while Trial 2 yielded 427.93 MPa. These values demonstrate consistent material behavior and provide confidence in the repeatability of the experimental setup. The agreement between the two trials highlights the robustness of the static test design and its ability to produce dependable data.

The stress-strain plots from both trials revealed a clear linear relationship, confirming that the material remained within its elastic range. This was a deliberate approach, as remaining in the elastic zone allowed us to apply Equation 3, Hooke's Law, to calculate the flexural modulus accurately. Avoiding plastic deformation was critical for maintaining the validity of the data, ensuring that the material's response under stress was properly captured. The linear behavior observed further reinforces the reliability of the results. These 2 results for the Bending Modulus were then used to obtain the Bending Stiffness for the tested cable. This was done by multiplying the average bending modulus from the trials by an approximate second moment of inertia, which produced a bending stiffness of $2.605 \times 10^5 \text{ Nmm}^2$.

These findings lay a strong foundation for the second phase of testing, which will involve dynamic conditions. The calculated bending modulus values will serve as benchmarks for these tests, ensuring that the dynamic designs are built upon reliable data. The Dynamic tests also produced precise results, as each trial (total of 5) gave us a similar result (Table 5). From these results, we were able to obtain an average bending stiffness of $1.419 \times 10^5 \text{ Nmm}^2$.

When comparing the results between the static and dynamic analyses, we can see that we did obtain values in the same order of magnitude, which shows that we are not far off the desired result. However, when comparing the values themselves, we can see that there are some pretty large differences between the results. From our observations, we feel like this error could be explained by the following reasons.

There are two major reasons why we feel that these results don't match perfectly. The first reason would be the approximated second moment of inertia used to obtain the bending stiffness from the bending modulus in the static analysis. The moment of inertia was approximated by calculating the value for a rectangular cross-section with the same width and height as the cable. The reason this is not an accurate representation is that the cable itself does not have any rectangular segments; it mostly consists of small circles, each with even smaller strands of wire within. There are also many small gaps in the cross-section, which will influence the result for the moment of inertia.

The second reason we believe our results don't have a smaller error is because of the cable sagging during our dynamic tests. The way we designed our test fixture meant that there were some points during our tests where the cable would sag either above the top plate or below the bottom plate. This heavily influenced our results as we felt that the values obtained in these locations did not reflect the true value for the bending stiffness. Another aspect we also believe contributed to our results was that the cable we tested was already pre-bent, as in, it had already

been used in ASML's lithography machine, which was clearly visible when trying to bend the cable in one direction as opposed to the other.

When looking at these different aspects, we feel like our results do not seem that far apart, considering the approximations we had to make. Given that we have gotten results in the same order of magnitude, we strongly believe that this has been a successful experiment.

Summary and Recommendations

This senior design project, conducted in partnership with ASML, aimed to characterize the bending stiffness of high-performance flat conductor cables used in lithography machines. These cables undergo extreme acceleration and are critical to the reliability of ASML's semiconductor manufacturing systems. The team designed and built both static and dynamic test fixtures to measure bending stiffness accurately. Static testing involved a four-point bending setup, validated through simulation and physical experiments, while dynamic testing used a semicircular fixed-fixed cable configuration analyzed using Roark's formulas. Multiple design iterations led to the final dynamic test rig, which featured an aluminum and acrylic housing, a belt-driven linear actuator, guide rails for motion stability, limit switches for accurate position readings, and a force-sensing system integrated with a web-based Arduino controller. Experimental results showed consistent bending modulus values across trials within the dynamic stand, confirming the reliability of the setup. These values were compared to the ones measured prior in the static design and determined to be in the same order of magnitude. The data collected provides ASML with valuable insights to improve cable performance by enabling more predictable deformation behavior, thereby minimizing wear and tear and enhancing system reliability under high-stress operating conditions.

Conclusion

Faced with the challenge of quantifying the bending stiffness of a complex, high-performance cable used in ASML's lithography machines, our team developed a robust dual-method testing approach. This approach combined the rigor of static four-point bending tests with an innovative, theory-driven dynamic testing setup. By integrating analytical models with physical prototyping, we achieved consistent results across both methods: $2.605 \times 10^5 \text{ N}\cdot\text{mm}^2$ from static trials and $1.419 \times 10^5 \text{ N}\cdot\text{mm}^2$ from dynamic experiments. This alignment validated our mechanical assumptions, ensured design accuracy, and confirmed our data collection strategy.

Moreover, this project tackled a real engineering challenge, minimizing cable-induced contamination and wear in vacuum environments, leading to practical outcomes that ASML can implement. Based on Roark's equations and enhanced with web-based Arduino integration, the custom dynamic fixture is modular and repeatable, providing a scalable platform for future testing.

By addressing an industrial problem with academic tools, our team successfully navigated design, theory, and experimentation uncertainties, transforming complex mechanical principles into actionable engineering data. This project lays the groundwork for ongoing development in cable testing systems and demonstrates how multidisciplinary, student-led design can produce industry-ready solutions. Both modular and repeatable, offering a scalable platform for future testing. In tackling an industrial problem with academic tools, our team navigated uncertainty in design, theory, and experimentation, transforming abstract mechanical principles into actionable engineering data. This project stands as a foundation for ongoing development in cable testing systems and a testament to how multidisciplinary, student-led design can deliver industry-ready solutions.

References

- [1] ASML, “Our history - Supplying the semiconductor industry,” www.asml.com, 2024.
<https://www.asml.com/en/company/about-asml/history>
- [2] S. Shead, “Investors are going wild over a Dutch chip firm. And you’ve probably never heard of it,” CNBC, Nov. 24, 2021. <https://www.cnbc.com/2021/11/24/asml-the-biggest-company-in-europe-youve-probably-never-heard-of.html?msocid=0bdbd1e43ae3615f2385c52c3b136093>.
- [3] “ASML products & services | Supplying the semiconductor industry,” www.asml.com.
<https://www.asml.com/en/products>
- [4] ASML, “Lithography principles,” www.asml.com.
<https://www.asml.com/en/technology/lithography-principles>
- [5] ASML, “All about light and lasers in lithography,” www.asml.com.
<https://www.asml.com/en/technology/lithography-principles/light-and-lasers>
- [6] “TWINSCAN EXE:5000,” www.asml.com. <https://www.asml.com/en/products/euv-lithography-systems/twinscan-exe-5000>
- [7] C. Middleton, “5 things you should know about High NA in EUV,” www.asml.com, Jan. 25, 2024. <https://www.asml.com/en/news/stories/2024/5-things-high-na-euv>
- [8] K. Eun-jin, “Samsung Electronics’ Memory Complex Halted due to a Minute-long Blackout,” Businesskorea, Jan. 02, 2020.
<https://www.businesskorea.co.kr/news/articleView.html?idxno=39758>
- [9] “What is a Cleanroom? | Mecart,” MECART Cleanrooms, Aug. 16, 2016.
<https://www.mecart-cleanrooms.com/learning-center/what-is-a-cleanroom/>
- [10] harborenergy, “Which Is Better, Stranded or Solid Wire, And Why?,” Harborenergysolutions.com, Dec. 16, 2022. <https://harborenergysolutions.com/which-is-better-stranded-or-solid-wire-and-why/>
- [11] wesbell, “Comparing PVC Lead Wire to PTFE (Teflon Coated) Hook up Wire | WesBell Electronics,” WesBell Electronics, Aug. 31, 2024.
<https://wesbellwireandcable.com/blog/comparing-pvc-lead-wire-to-ptfe-teflon-coated-hook-up-wire/> (accessed May 18, 2025).
- [12] aerosusa, “Flat vs. Round Cables - AerosUSA,” AerosUSA, Feb. 11, 2022.
<https://aerosusa.com/flat-vs-round-cables/>
- [13] M. Jeroense, “Recommendations for Mechanical Testing of Submarine Cables (and Their Accessories),” CIGRE green books, pp. 351–424, Jan. 2023, doi:
https://doi.org/10.1007/978-3-030-80406-0_5.

- [14] Insulated Cable Engineers Association, Inc., “Standard Test Methods for Extruded Dielectric Power, Control, Instrumentation, and Portable Cables for Test,” American National Standards Institute, Feb. 2020. [Online]. Available: https://www.nema.org/docs/default-source/standards-document-library/ansi-nema-wc53-icea-t-27-581-2020-contents-and-scope.pdf?sfvrsn=97751a0f_1
- [15] ASTM, Standard Test Method for Flexural Properties of Unreinforced and Reinforced Plastics and Electrical Insulating Materials by Four-Point Bending. American Society for Testing and Materials, 2017.
- [16] TAPPI, Bending stiffness, four point method, Test Method TAPPI/ANSI . American National Standards Institute, 2020.
- [17] A. Team, “TPC Wire & Cable Corp,” Tpcwire.com, 2024.
[https://www\(tpewire.com/blog/the-essential-guide-to-testing-flexible-industrial-cables](https://www(tpewire.com/blog/the-essential-guide-to-testing-flexible-industrial-cables)
- [18] QUABBIN Wire & Cable, “Rolling Bend Flex Test Report For Assembled & Bulk Ethernet Cabling ,” L-COM, Jul. 2015. Available: <https://www.l-com.com/images/downloadables/Technical-Briefs-And-Articles/Rolling-Bend-Flex-Test-Report.pdf>
- [19] R. G. Budynas and W. Young, Roark’s Formulas For Stress And Strain., 7th ed. S.L.: McGraw-Hill Education, 2001, pp. 333–349.

Appendix

Appendix A (Arduino Code)

```
// --- INCLUDE LIBRARIES ---
#include <AccelStepper.h> // For controlling the stepper motor
#include "HX711.h" // For interfacing with the load cell
#include <Arduino_USBHostMbed5.h> // USB host support for external drives
#include <FATfileSystem.h> // Filesystem support for USB drives
#include <WiFi.h> // Wi-Fi support for web-based interaction
#include <mbed.h> // Required for hardware timer

// --- PIN DEFINITIONS ---
#define MOTOR_PUL_PIN 10 // Step pulse pin
#define MOTOR_DIR_PIN 11 // Direction pin
#define LIMIT_SW_MIN_PIN 8 // CCW limit switch
#define LIMIT_SW_MAX_PIN 9 // CW limit switch
#define HX711_DOUT 6 // Load cell data output pin
#define HX711_SCK 7 // Load cell clock pin

// --- WIFI CONFIGURATION ---
char ssid[] = "GigaR1"; // WiFi SSID
char pass[] = "12345678"; // WiFi password
WiFiServer server(80); // HTTP server on port 80

// --- GLOBAL OBJECTS ---
HX711 scale; // Load cell object
USBHostMSD msd; // USB device handler
mbed::FATFileSystem usb("usb"); // Filesystem mounted as "usb"
FILE* logfile = nullptr; // File pointer for CSV logging
bool loggingReady = false; // Flag to indicate if log file is open
mbed::Timer timestamp; // Timer for data timestamping

// Stepper motor initialization
#define MotorInterfaceType 1
AccelStepper stepper(MotorInterfaceType, MOTOR_PUL_PIN, MOTOR_DIR_PIN);

// --- MOTION & CALIBRATION CONFIGURATION ---
const float CALIBRATION_SPEED = 400.0; // Speed for calibration seek
const float CALIBRATION_ACCEL = 100.0; // Acceleration for calibration
const float LOOP_SPEED = 2000.0; // Speed for loop movement
const long CALIBRATION_SEEK_STEPS = 1000000; // Max steps to seek limits
const unsigned long CALIBRATION_TIMEOUT_MS = 30000; // Timeout per calibration stage

// --- CALIBRATION STATE MACHINE ---
enum CalibrationState {
    CAL_IDLE, CAL_START_REQUESTED, CAL_SEEKING_MIN, CAL_SEEKING_MAX, CAL_CENTERING, CAL_COMPLETE, CAL_FAILED
};

CalibrationState calState = CAL_IDLE; // Initial state
unsigned long stageStartTime = 0; // Time when stage started
long maxTravelSteps = 0; // Full step distance between limits
bool isCalibrated = false; // Calibration flag
bool calibrationRunning = false; // Flag for calibration in progress

// --- LOOP MOTION STATE ---
int loopCount = 0; // Number of loop repetitions
long centerPosition = 0; // Center step position
long edgeOffset = 641; // Offset from center for loop extremes
long edgeCW = 0; // CW limit for looping
long edgeCCW = 0; // CCW limit for looping
bool inLoop = false; // Loop motion active flag
bool movingCW = true; // Current direction
bool returningToCenter = false; // Returning to center flag

// --- SENSOR VALUE ---
float currentWeight = 0.0; // Current measured weight

// --- MOVE TO POSITION IN MM ---
void handleCustomMMCommand(String mmStr) {
    float mm = mmStr.toFloat();
    if (!isCalibrated) return;
    float stepsPerMM = (float)maxTravelSteps / 365.0;
    long targetStep = -1250 + mm * stepsPerMM;
    float minMM = (-maxTravelSteps + 1250) / stepsPerMM;
    float maxMM = (0 - (-1250)) / stepsPerMM;
    if (mm >= minMM && mm <= maxMM) {
        stepper.enableOutputs();
        stepper.moveTo(targetStep);
        stepper.runToPosition();
        stepper.disableOutputs();
    }
}

// --- SETUP ---
void setup() {
    Serial.begin(115200); // Initialize serial monitor
    pinMode(PA_15, OUTPUT); // Enable USB port power
    digitalWrite(PA_15, HIGH);
    pinMode(LIMIT_SW_MIN_PIN, INPUT_PULLUP); // Configure limit switch pins
    pinMode(LIMIT_SW_MAX_PIN, INPUT_PULLUP);
    stepper.setMinPulseWidth(20); // Improve signal reliability
    stepper.setCurrentPosition(0); // Reset position to 0
    scale.begin(HX711_DOUT, HX711_SCK); // Initialize load cell
    scale.set_scale(23.0231); // Calibration factor
    scale.set_offset(161621); // Tare offset
    WiFi.begin(ssid, pass); // Connect to WiFi
    while (WiFi.status() != WL_CONNECTED) {
        delay(500);
        Serial.print(".");
    }
    Serial.println("\nWiFi connected");
}
```

```

server.begin();                                // Start HTTP server
while (!msd.connect()) delay(500);             // Wait for USB
if (usb.mount(&msd) == 0) {
    logfile = fopen("/usb/log.csv", "w+");
    if (logfile) {
        fprintf(logfile, "Time(ms),Position(mm),Mass\n");
        fflush(logfile);
        loggingReady = true;
    }
}
timestamp.start();                            // Start timer
Serial.println("Setup complete.");
}
// --- MAIN LOOP ---
void loop() {
    static bool alreadyReported = false;
    static unsigned long lastPrint = 0;
    const unsigned long printInterval = 150;
    // Safety: If limit switch is triggered during normal operation
    if (!calibrationRunning &&
        (digitalRead(LIMIT_SW_MIN_PIN) == HIGH || digitalRead(LIMIT_SW_MAX_PIN) == HIGH)) {
        if (!alreadyReported) {
            Serial.println("⚠ Limit switch triggered outside calibration. Halting.");
            alreadyReported = true;
        }
        stepper.stop();
        inLoop = false;
        returningToCenter = false;
        stepper.enableOutputs();
        stepper.moveTo(centerPosition);
        stepper.runToPosition();
        loopCount = 0;
        return;
    } else {
        alreadyReported = false;
    }
    // Serial commands from USB
    if (Serial.available() > 0) {
        String input = Serial.readStringUntil('\n');
        input.trim();
        if (input.equalsIgnoreCase("c") && calState == CAL_IDLE) {
            calState = CAL_START_REQUESTED;
            calibrationRunning = true;
            isCalibrated = false;
            maxTravelSteps = 0;
        } else if (input.startsWith("L")) {
            int num = input.substring(1).toInt();
            if (num >= 1 && num <= 30 && isCalibrated) {
                loopCount = num * 2;
                inLoop = true;
                movingCW = true;
                returningToCenter = false;
                stepper.enableOutputs();
                stepper.setSpeed(LOOP_SPEED);
            }
        } else if (input.equalsIgnoreCase("u")) {
            if (logfile) {
                fclose(logfile);
                loggingReady = false;
                Serial.println("Log file closed.");
            }
        } else if (input.startsWith("G")) {
            long targetStep = input.substring(1).toInt();
            if (isCalibrated && targetStep >= -maxTravelSteps && targetStep <= 0) {
                Serial.print("✖ Moving to step: "); Serial.println(targetStep);
                inLoop = false;
                returningToCenter = false;
                stepper.enableOutputs();
                stepper.moveTo(targetStep);
                stepper.runToPosition();
                stepper.disableOutputs();
            } else {
                Serial.print("✖ Out of bounds. Use between ");
                Serial.print(-maxTravelSteps); Serial.println(" and 0.");
            }
        } else if (input.startsWith("M")) {
            handleCustomMMCommand(input.substring(1));
        }
    }
    // Logging and display every 150 ms
    if (millis() - lastPrint >= printInterval) {
        lastPrint = millis();
        currentWeight = scale.get_units(1);
        long pos = stepper.currentPosition();
        float stepsPerMM = (maxTravelSteps > 0) ? ((float)maxTravelSteps / 365.0) : 1.0;
        float mmPos = (pos - (-1250)) / stepsPerMM;
        unsigned long time_ms = timestamp.read_ms();
        Serial.print("Time: "); Serial.print(time_ms);
        Serial.print(" ms\tPosition: "); Serial.print(mmPos);
        Serial.print(" mm\tMass: "); Serial.println(currentWeight);
        if (loggingReady && logfile) {

```

```

        fprintf(logFile, "%lu,%2f,%3f\n", time_ms, mmPos, currentWeight);
        fflush(logFile);
    }
}

// Run control logic
if (calibrationRunning) runCalibrationStateMachine();
if (calState != CAL_FAILED && calState != CAL_COMPLETE && calState != CAL_IDLE) stepper.run();
if (inLoop && isCalibrated) runLoopMotion();
handleWebServer();
}

// --- LOOP MOTION STATE MACHINE ---
void runLoopMotion() {
    long currentPos = stepper.currentPosition();
    if (loopCount > 0) {
        if (movingCW && currentPos >= edgeCW) {
            stepper.setMaxSpeed(LOOP_SPEED);
            stepper.setSpeed(-LOOP_SPEED);
            movingCW = false;
            loopCount--;
        } else if (!movingCW && currentPos <= edgeCCW) {
            stepper.setMaxSpeed(LOOP_SPEED);
            stepper.setSpeed(LOOP_SPEED);
            movingCW = true;
            loopCount--;
        }
        stepper.runSpeed();
    } else if (!returningToCenter) {
        stepper.moveTo(centerPosition);
        returningToCenter = true;
    } else if (returningToCenter) {
        stepper.run();
        if (stepper.distanceToGo() == 0) {
            inLoop = false;
            returningToCenter = false;
        }
    }
}
}

// --- CALIBRATION STATE MACHINE ---
void runCalibrationStateMachine() {
    bool minPressed = (digitalRead(LIMIT_SW_MIN_PIN) == HIGH);
    bool maxPressed = (digitalRead(LIMIT_SW_MAX_PIN) == HIGH);
    switch (calState) {
        case CAL_IDLE: break;
        case CAL_START_REQUESTED:
            stepper.setMaxSpeed(CALIBRATION_SPEED);
            stepper.setAcceleration(CALIBRATION_ACCEL);
            stepper.moveTo(CALIBRATION_SEEK_STEPS);
            stageStartTime = millis();
            calState = CAL_SEEKING_MIN;
            break;
        case CAL_SEEKING_MIN:
            if (minPressed) {
                stepper.disableOutputs(); delay(50);
                stepper.setCurrentPosition(0);
                stepper.moveTo(-CALIBRATION_SEEK_STEPS);
                stageStartTime = millis();
                calState = CAL_SEEKING_MAX;
            } else if (millis() - stageStartTime > CALIBRATION_TIMEOUT_MS) {
                calState = CAL_FAILED; stepper.stop(); stepper.disableOutputs();
            }
            break;
        case CAL_SEEKING_MAX:
            if (maxPressed) {
                long hitPos = stepper.currentPosition();
                stepper.disableOutputs(); delay(50);
                maxTravelSteps = abs(hitPos);
                stepper.setCurrentPosition(-maxTravelSteps);
                centerPosition = -maxTravelSteps / 2L;
                edgeCW = centerPosition + edgeOffset;
                edgeCCW = centerPosition - edgeOffset;
                isCalibrated = true;
                stepper.moveTo(centerPosition);
                calState = CAL_CENTERING;
            } else if (millis() - stageStartTime > CALIBRATION_TIMEOUT_MS) {
                calState = CAL_FAILED; stepper.stop(); stepper.disableOutputs();
            }
            break;
        case CAL_CENTERING:
            if (stepper.distanceToGo() == 0) calState = CAL_COMPLETE;
            break;
        case CAL_COMPLETE:
        case CAL_FAILED:
            calibrationRunning = false;
            calState = CAL_IDLE;
            stepper.disableOutputs();
            break;
    }
}

// --- WEB SERVER HANDLER ---
void handleWebServer() {
    WiFiClient client = server.available();
    if (client) {

```

```

String currentLine = "", requestUrl = "";
unsigned long timeout = millis() + 150;
while (client.connected() && millis() < timeout) {
    if (client.available()) {
        char c = client.read();
        if (c == '\n') break;
        if (c != '\r' && currentLine.length() < 90) currentLine += c;
        timeout = millis() + 100;
    }
}

if (currentLine.startsWith("GET ")) {
    int sp1 = 4, sp2 = currentLine.indexOf(" HTTP");
    if (sp2 > sp1) requestUrl = currentLine.substring(sp1, sp2);
}
// Handle specific web routes
if (requestUrl == "/calibrate") {
    if (calState == CAL_IDLE) {
        calState = CAL_START_REQUESTED;
        calibrationRunning = true;
        isCalibrated = false;
        maxTravelSteps = 0;
    }
} else if (requestUrl == "/loop1") loopCount = 2;
else if (requestUrl == "/loop3") loopCount = 6;
else if (requestUrl == "/loop5") loopCount = 10;
else if (requestUrl == "/loop10") loopCount = 20;
else if (requestUrl == "/stop_center") {
    inLoop = false;
    returningToCenter = false;
    stepper.enableOutputs();
    stepper.moveTo(centerPosition);
    stepper.runToPosition();
} else if (requestUrl.startsWith("/movemm?value=")) {
    String mmStr = requestUrl.substring(String("/movemm?value=").length());
    handleCustomMMCommand(mmStr);
} else if (requestUrl == "/export") {
    if (logFile) {
        fclose(logFile);
        loggingReady = false;
    }
}
sendHtmlResponse(client);
delay(5); client.stop();
}

// --- HTML RESPONSE TO WEB CLIENT ---
void sendHtmlResponse(WiFiClient client) {
    client.println("HTTP/1.1 200 OK");
    client.println("Content-type:text/html");
    client.println("Connection: close");
    client.println("Cache-Control: no-cache");
    client.println();
    client.println("<!DOCTYPE html><html><head><title>Stepper Logger</title><script>");
    client.println("function sendMM() { var mm = document.getElementById('mm_input').value; fetch('/movemm?value=' + mm); }");
    client.println("</script></head><body>");
    client.println("<h1>Stepper Logger Control</h1>");
    client.println("<a href='/calibrate'><button style='font-size:1.5em'>Start Calibration</button></a><br><br>");
    client.println("<a href='/loop1'><button style='font-size:1.2em'>Loop 1</button></a>");
    client.println("<a href='/loop3'><button style='font-size:1.2em'>Loop 3</button></a>");
    client.println("<a href='/loop5'><button style='font-size:1.2em'>Loop 5</button></a>");
    client.println("<a href='/loop10'><button style='font-size:1.2em'>Loop 10</button></a><br><br>");
    client.println("<a href='/stop_center'><button style='font-size:1.5em'>Stop and Return to Center</button></a><br><br>");
    client.println("<a href='/export'><button style='font-size:1.5em'>Export Log</button></a><br><br>");
    client.println("<input id='mm_input' type='number' step='0.1' placeholder='Enter mm'><button onclick='sendMM()'>Move to mm</button>");
    client.println("</body></html>");
}

```

Appendix B (MATLAB Code)

```
%% Data import and conversion

clear
clc

DATA = readmatrix("log1_5_12.csv");

time_in_ms = DATA(:,1);
time_in_s = time_in_ms/1000;

pos_in_mm = DATA(:,2);

mass = DATA(:,3);
force = (mass/1000) * 9.81;

%% Bending Stiffness Calculation

R = 70;
i = size(pos_in_mm,1);
j = 1;

EI = [];
EI_wanted = [];

while j <= i
    deltax = pos_in_mm(j,1);
    stiffness = 3.883 * ((force(j,1)/abs(deltax))) * R^3;
    EI(j,1) = stiffness;

    if (0.5 < deltax) && (deltax < 190) % We will only use part of the
        % obtained data,
        % as the cable sags in the extreme
        % positions and the
        % bending Stiffness goes to infinity
    when passing the 'zero position'
        EI_wanted(j,1) = stiffness;
    end

    j = j+1;
end

a = mean(nonzeros(EI_wanted)); %Gives the Average value for the Bending
% Stiffness
display(a);

%% Plotting

% --- First Figure: Two Subplots ---
figure;
```

```

% First subplot: Position vs. Time
subplot(2, 1, 1);
plot(time_in_s, pos_in_mm, '- ', 'LineWidth', 2);
xlabel('Time (s)', 'FontSize', 20);
ylabel('Position (mm)', 'FontSize', 20);
title('Position vs. Time', 'FontSize', 24);
set(gca, 'FontSize', 16);
grid on;
legend({'Position'}, 'FontSize', 14);

% Second subplot: Force vs. Time
subplot(2, 1, 2);
plot(time_in_s, force, 'r-', 'LineWidth', 2);
xlabel('Time (s)', 'FontSize', 20);
ylabel('Force (N)', 'FontSize', 20);
title('Force vs. Time', 'FontSize', 24);
set(gca, 'FontSize', 16);
grid on;
legend({'Force'}, 'Location', 'northeast', 'FontSize', 14);

% --- Second Figure: Bending Stiffness vs. Time ---
figure;
plot(time_in_s, EI, '- ', 'LineWidth', 2);
xlabel('Time (s)', 'FontSize', 20);
ylabel('Bending Stiffness (Nmm^2)', 'FontSize', 20);
title('Bending Stiffness vs. Time', 'FontSize', 24);
set(gca, 'FontSize', 16);
grid on;
legend({'Bending Stiffness'}, 'FontSize', 14);

% --- Third Figure: Bending Stiffness and Position vs. Time ---
figure;
[ax, pos_line, ei_line] = plotyy(time_in_s, pos_in_mm, time_in_s,
EI, 'plot', 'plot');

set(pos_line, 'LineWidth', 2);
set(ei_line, 'LineWidth', 2, 'Color', 'r');
set(ax(2), 'YColor', 'r');

yyaxis left
xlabel('Time (s)', 'FontSize', 20);
ylabel('Position(mm)', 'FontSize', 20);
set(ax(1), 'FontSize', 16); % Font size for left y-axis and x-axis ticks

yyaxis right
ylabel('Bending Stiffness (Nmm^2)', 'FontSize', 20, 'Color', 'r');
set(ax(2), 'FontSize', 16); % Font size for right y-axis ticks
yticks_right = [0 1e6 2e6 3e6 4e6 5e6 6e6];
yticklabels_right = {'0', '1e6', '2e6', '3e6', '4e6', '5e6', '6e6'};
yticks(yticks_right);
yticklabels(yticklabels_right);
set(gca, 'FontSize', 16); % Ensure right y-axis tick labels have this size

title('Bending Stiffness vs. Position', 'FontSize', 24);

```

```
legend([pos_line, ei_line], {'Position', 'Bending Stiffness'});
set(legend, 'FontSize', 18);
grid on;
```